

The PDE-Constrained Optimization Method Based on MFS for Solving Inverse Heat Conduction Problems

Yongfu ZHANG^{1,2}, Chongjun LI^{1,*}

1. School of Mathematical Sciences, Dalian University of Technology, Liaoning 116024, P. R. China;

2. College of Mathematics, Inner Mongolia University for Nationalities,

Inner Mongolia 028043, P. R. China

Abstract In this paper, we present an effective meshless method for solving the inverse heat conduction problems, with the Neumann boundary condition. A PDE-constrained optimization method is developed to get a global approximation scheme in both spatial and temporal domains, by using the fundamental solution of the governing equation as the basis function. Since the initial measured data contain some noises, and the resulting systems of equations are usually ill-conditioned, the Tikhonov regularization technique with the generalized cross-validation criterion is applied to obtain more stable numerical solutions. It is shown that the proposed schemes are effective by some numerical tests.

Keywords inverse heat conduction problem; PDE-constrained optimization; method of fundamental solutions; time-dependent heat source term; Tikhonov regularization method

MR(2010) Subject Classification 65M32; 65F22; 65L60; 35Q93

1. Introduction

In heat conduction problems, when the heat flux and/or temperature histories on the surface of a solid body are known as functions of time, furthermore, the temperature distribution can be found. This is called a direct problem. But in many heat transfer settings, the surface heat flux and temperature histories have to be determined from temperature measurements at one or more interior locations. This is termed as an inverse problem [1]. Inverse heat conduction problems (IHCPs) play very important role in many fields of engineering technology and computational science, which have been widely investigated over the last 40 years. Many researchers have been attracted attention to study IHCPs, including heat flux, material structure control [2], industrial controlling-models with heat propagation, and mechanics of continuous media etc in related areas [3]. However, IHCPs are more difficult to solve than the direct heat conduction problems, because they are usually extremely sensitive to the measured noisy data, it means that IHCPs are ill-posed in the sense of Hadamard [4], i.e., any small perturbation of measurement values

Received July 6, 2017; Accepted August 4, 2017

Supported by the National Natural Science Foundation of China (Grant Nos.11290143; 11471066; 11572081), the Fundamental Research of Civil Aircraft (Grant No.MJ-F-2012-04), the Fundamental Research Funds for the Central Universities (Grant No.DUT15LK44) and the Scientific Research Funds of Inner Mongolia University for the Nationalities (Grant No.NMD1304).

* Corresponding author

E-mail address: chongjun@dlut.edu.cn (Chongjun LI)

can lead to enormous error for computing the identified solutions, and the resulting matrix is usually ill-conditioned, thus the key is to find some special numerical techniques to overcome the ill-posedness of problems, further to get stable and accurate numerical solutions. Although heat conduction process is very smooth, it is shown that the process is irreducible to IHCPs. It means that the characteristics of the problem solutions may not be affected by the observed data, it is one of the major difficulties of IHCPs [3,5,6].

In practice, many traditional numerical methods for solving one-dimensional and multi-dimensional IHCPs have been proposed during the last decades, such as the finite difference method (FDM) and the finite element method (FEM) [7]. However, the above methods confine to solve the problems possessing very special regular domains and low-dimensional cases, moreover, the property of mesh-dependent requires enormous computation cost for lots of grids or elements, so it can derive numerical instability. In addition, the boundary element method (BEM) does not require domain discretization, which only need boundary discretization, the measured data of temperature can be chosen in an arbitrary way, and it does not need any internal cells [8–10]. In contrast to a meshless method, the BEM would suffer costly numerical integrations high-dimensional irregular domain [11].

Meshless methods have been proposed and effectively employed to solve many problems in engineering and science, the major advantage of meshless methods can easily solve high-dimensional IHCPs with arbitrary geometry, it can directly apply the geometry of domain to avoid lots of computation difficulties, such as mesh generation, re-meshing and other data-dependent techniques, since the meshless methods are mesh-independent [5,12–14]. In this setting, a class of meshless methods is focused on the use of radial basis functions (RBFs) for solving partial differential equations (PDEs) [15,16]. In addition, many numerical methods by using RBFs have been developed to solve one-dimensional and multi-dimensional IHCPs [17–19]. Recently, a meshless method based on the fundamental solution and radial basis function was presented to solve IHCP [20]. In [21], Zhang and Li proposed a Gaussian RBFs method with regularization to solve IHCPs, with the Neumann boundary conditions. In scientific computation and simulation, the method of fundamental solutions (MFS) is an integration-free and meshless boundary collocation method for solving IHCPs [3,5,22–24], which belongs to the family of Trefftz methods, and proposed primarily by Kupradze and Alexdze during the early 1960s (see [25]). Recently, Chen et al. [26] applied MFS to characterize the space-dependent thermal conductivity of nonlinear functionally graded materials (FGMs). Sun [27] proposed a meshless method based on MFS for solving the steady-state heat conduction. Additionally, in recent several years, some effective methods have attracted considerable attention for the conjunction of PDE-constrained optimization, meshless techniques and multigrid algorithms etc. to solve the distribution control problems [28–31].

In this paper, we develop a general form of the PDE-constrained optimization method for solving a class of IHCPs, with the Neumann boundary condition and the time-dependent heat source term, which is an effective meshless numerical technique. Compared with the mesh-dependent techniques, such as FDM and FEM, the developed method does not require any

discrete boundary or domain, by using the collocation technique in the given physical domain, it can obtain a global approximation solution in both the spatial and temporal domains. Meanwhile, due to the use of fundamental solution, it can be reduced the computation complexity by avoiding computation of the Lagrange multiplier term.

The paper is organized as follows. In Section 2, we consider a class of IHCPs with the time-dependent heat source term $f(t)$ and the Neumann boundary condition. The PDE-constrained optimization technique based on MFS is concretely presented in Section 3, involving 1-D IHCP for the rectangular domain, 2-D IHCP for the rectangular domain and 2-D IHCP for the non-rectangular domain with smooth boundary cases, respectively. In order to test the accuracy and efficiency of the presented approaches, several numerical examples are given in Section 4. Finally, we conclude the paper in Section 5.

2. Statement of the IHCPs

We consider the following heat conduction equation with time-dependent heat source $f(t)$:

$$u_t(x, t) = \Delta u(x, t) + f(t), \quad (x, t) \in \Omega \times (0, t_{\max}], \tag{2.1}$$

with the initial condition

$$u(x, 0) = \varphi(x), \quad x \in \bar{\Omega}, \tag{2.2}$$

the Neumann boundary condition

$$\frac{\partial u}{\partial \bar{n}}(x, t) = s(x, t), \quad (x, t) \in \partial\Omega \times [0, t_{\max}], \tag{2.3}$$

and the over-specification point x^* in the given domain Ω satisfying

$$u(x^*, t) = g(t), \quad t \in [0, t_{\max}], \tag{2.4}$$

where Ω is a simply connected domain in \mathbb{R}^d ($d=1, 2$ or 3), \bar{n} is the unit outward normal vector to $\partial\Omega$, Δ denotes the Laplace operator, $\bar{\Omega}$ and $\partial\Omega$ indicate the closure and boundary of Ω respectively, $\partial u/\partial \bar{n}$ is referred to as the directional derivative in the direction normal to $\partial\Omega$. Simultaneously, the functions $\varphi(x)$, $s(x, t)$ and $g(t)$ are known, but $u(x, t)$ and $f(t)$ are identified in Eqs. (2.1)–(2.4). Since the governing Eq. (2.1) involves two unknown functions $u(x, t)$ and $f(t)$, we here adopt the following integral transformation, which transforms Eq. (2.1) into another homogeneous equation. Similar transformations can be found in [17,18,21,22].

Let

$$r(t) = \int_0^t f(\eta) d\eta, \tag{2.5}$$

and

$$v(x, t) = u(x, t) - r(t). \tag{2.6}$$

Thus Eqs. (2.1)–(2.3) can be transformed into the following formulas

$$v_t(x, t) = \Delta v(x, t), \quad (x, t) \in \Omega \times (0, t_{\max}], \tag{2.7}$$

with the initial condition

$$v(x, 0) = \varphi(x), \quad x \in \bar{\Omega}, \quad (2.8)$$

and the Neumann boundary condition

$$\frac{\partial v}{\partial \bar{n}}(x, t) = s(x, t), \quad (x, t) \in \partial\Omega \times [0, t_{\max}]. \quad (2.9)$$

According to the Eqs. (2.4)–(2.6), we can obtain $r(t)$, $f(t)$ as follows

$$r(t) = g(t) - v(x^*, t), \quad (2.10)$$

$$f(t) = r_t(t). \quad (2.11)$$

3. PDE-constrained optimization by MFS

In this section, we take the L^2 -norm defined in the domain $\Omega \times [0, t_{\max}]$. Eqs. (2.7)–(2.9) above can be considered as a boundary distributed control problem, more details may be found in [28–31]. It means that the cost functional gets to minimize, which is derived from the initial and Neumann boundary conditions. Further, the Eqs. (2.7)–(2.9) can be formulated as the following constrained optimization problem. In practice, the obtained measurement data often contain some errors from the initial and boundary measured values, thus we have

$$\min_v \mathcal{J}(v) := \frac{1}{2} \left\{ \|v(x, 0) - \varphi^\sigma(x)\|_{L^2(\bar{\Omega})}^2 + \left\| \frac{\partial v}{\partial \bar{n}}(x, t) - s^\sigma(x, t) \right\|_{L^2(\partial\Omega \times [0, t_{\max}])}^2 \right\}, \quad (3.1)$$

subject to

$$v_t(x, t) = \Delta v(x, t), \quad (x, t) \in \Omega \times (0, t_{\max}]. \quad (3.2)$$

Here, the Eqs. (3.1) and (3.2) would be solved by applying the Lagrange multiplier method in the sense of unconstrained optimization, so the Lagrangian for the problems (3.1) and (3.2) is defined by

$$\begin{aligned} \mathcal{L}(v, \lambda) = & \frac{1}{2} \left\{ \|v(x, 0) - \varphi^\sigma(x)\|_{L^2(\bar{\Omega})}^2 + \left\| \frac{\partial v}{\partial \bar{n}}(x, t) - s^\sigma(x, t) \right\|_{L^2(\partial\Omega \times [0, t_{\max}])}^2 \right\} + \\ & \lambda \|v_t(x, t) - \Delta v(x, t)\|_{L^2(\Omega \times (0, t_{\max}])}^2, \end{aligned} \quad (3.3)$$

where σ denotes the noise level of input data involving in the initial and Neumann boundary conditions respectively, and λ is a Lagrange multiplier. Mathematically, the purpose of the Lagrange multiplier method is to find the global minimum of (3.3) (the convex functional) with respect to the variables v and λ . Thus, we consider the following optimization problem

$$(v^*, \lambda^*) := \arg \min_{v, \lambda} \mathcal{L}(v, \lambda), \quad (3.4)$$

where (v^*, λ^*) is a pair of stationary point for the Lagrange functional $\mathcal{L}(v, \lambda)$. In general, it would be infeasible to obtain directly the above values v^* , λ^* in the formula (3.4) by computing the partial derivative of \mathcal{L} , here, the identified function v^* contains both the spatial and time variables. In addition, if the boundary conditions are complex, the usual approach is to discretize the boundary into linear segments, and apply numerical schemes to solve problem [32].

In order to deal with the problem (3.4), the approximation solution $\tilde{v}(x, t)$ of the exact $v(x, t)$ is constructed by using the fundamental solution of the given heat equation as basis function, so the scheme can lead to a global approximation in both the spatial and temporal domains. The fundamental solution of Eq. (2.7) (see [3,5]) is presented by

$$F(x, t) = (4\pi t)^{-\frac{d}{2}} \exp\left(-\frac{\|x\|^2}{4t}\right)H(t),$$

where $H(t)$ is the Heaviside function, $\|\cdot\|$ indicates the Euclidean norm, and d denotes the d -dimensional Euclidean space in this paper. Suppose $T > t_{\max}$ is a constant, a general solution of (2.7) in domain $\Omega \times (0, t_{\max}]$ is given by

$$\phi(x, t) = F(x, t + T).$$

The time shift function $\phi(x, t)$ as the basis function is applied to represent the approximation solution of v as follows

$$\tilde{v}(x, t) = \sum_{i=1}^N \alpha_i \phi_i(x, t), \tag{3.5}$$

where $\phi_i(x, t) = \phi(x - x_i^s, t - t_i^s)$, and $\{\alpha_i\}_{i=1}^N$ are unknown coefficients to be determined. Let $\Theta := \{(x_i^s, t_i^s) \in \mathbb{R}^d \times \mathbb{R} : i = 1, 2, \dots, N\}$ be the chosen source points, which are located outside the physical domain to overcome the singularity of fundamental solution [3,5,22]. Combining with Eqs. (3.3) and (3.5), we further get

$$\begin{aligned} \tilde{\mathcal{L}}_1(\Lambda, \lambda, x, t) = & \frac{1}{2} \left\{ \left\| \sum_{i=1}^N \alpha_i \phi_i(x, 0) - \varphi^\sigma(x) \right\|_{L^2(\bar{\Omega})}^2 + \right. \\ & \left. \left\| \sum_{i=1}^N \alpha_i \frac{\partial \phi_i}{\partial \bar{n}}(x, t) - s^\sigma(x, t) \right\|_{L^2(\partial\Omega \times [0, t_{\max}])}^2 \right\} + \\ & \lambda \left\| \sum_{i=1}^N \alpha_i \left(\frac{\partial \phi_i}{\partial t}(x, t) - \Delta \phi_i(x, t) \right) \right\|_{L^2(\Omega \times (0, t_{\max}])}^2, \end{aligned} \tag{3.6}$$

where $\Lambda = (\alpha_1, \alpha_2, \dots, \alpha_N)'$, the superscript $'$ denotes the transpose of a vector or matrix. According to the property of fundamental solution, which can automatically satisfy the governing Eqs. (2.7) and (3.2) in the domain $\Omega \times (0, t_{\max}]$, the following form holds

$$\frac{\partial \phi_i}{\partial t}(x, t) - \Delta \phi_i(x, t) \equiv 0, \quad (x, t) \in \Omega \times (0, t_{\max}], \tag{3.7}$$

then we can write Eq. (3.6) by the formula (3.7) as follows

$$\begin{aligned} \tilde{\mathcal{L}}_2(\Lambda, x, t) = & \frac{1}{2} \left\{ \left\| \sum_{i=1}^N \alpha_i \phi_i(x, 0) - \varphi^\sigma(x) \right\|_{L^2(\bar{\Omega})}^2 + \right. \\ & \left. \left\| \sum_{i=1}^N \alpha_i \frac{\partial \phi_i}{\partial \bar{n}}(x, t) - s^\sigma(x, t) \right\|_{L^2(\partial\Omega \times [0, t_{\max}])}^2 \right\}. \end{aligned} \tag{3.8}$$

In practice, we often obtain some discrete measurement data of functions $\varphi^\sigma(x)$ and $s^\sigma(x, t)$, so the integral implementation of $\tilde{\mathcal{L}}_2(\Lambda, x, t)$, in L^2 -norm sense, would fail and be infeasible to

solve directly. In order to solve the problem (3.8) numerically, we here apply the “optimize-discretize-optimize” method in this paper, i.e., the optimality condition is derived firstly, then the form is discretized, and last the unknown parameters are determine by using the optimization scheme. We can refer to the literatures [28,29] for the optimize-discretize and discretize-optimize methods.

Let $\Xi := \{(x_j, t_j) \in \mathbb{R}^d \times \mathbb{R} : j = 1, 2, \dots, M\}$ be the chosen collocation points on the physical boundary, the Eq. (3.8) can be simplified by using the collocation technique as follows

$$\tilde{\mathcal{L}}_3(\Lambda) = \frac{1}{2} \left\{ \sum_{j=1}^{m_1} \left(\sum_{i=1}^N \alpha_i \phi_i(x_j, 0) - \varphi^\sigma(x_j) \right)^2 + \sum_{j=m_1+1}^M \left(\sum_{i=1}^N \alpha_i \frac{\partial \phi_i}{\partial \bar{n}}(x_j, t_j) - s^\sigma(x_j, t_j) \right)^2 \right\}. \quad (3.9)$$

Let us consider the minimization of quadratic problem (3.9) to determine Λ by

$$\Lambda^* := \arg \min_{\Lambda} \tilde{\mathcal{L}}_3(\Lambda), \quad (3.10)$$

where $\Lambda^* = (\alpha_1^*, \alpha_2^*, \dots, \alpha_N^*)'$, and the identified coefficients Λ^* can be obtained by solving a system of linear equations. For more details one can see the following subsections 3.1-3.3. Furthermore, the approximation solution \tilde{v} of v to the problems (2.7)–(2.9) is developed by

$$\tilde{v}(x, t) = \sum_{i=1}^N \alpha_i^* \phi_i(x, t), \quad (3.11)$$

and, we have

$$\tilde{r}(t) = g(t) - \sum_{i=1}^N \alpha_i^* \phi_i(x^*, t), \quad (3.12)$$

$$\tilde{u}(x, t) = g(t) + \sum_{i=1}^N \alpha_i^* (\phi_i(x, t) - \phi_i(x^*, t)). \quad (3.13)$$

Suppose $g(t) \in C^1[0, t_{\max}]$, we get

$$\tilde{f}(t) = g_t(t) - \sum_{i=1}^N \alpha_i^* \frac{\partial \phi_i}{\partial t}(x^*, t). \quad (3.14)$$

If the function $g(t)$ is not differentiable in the interval $[0, t_{\max}]$ with respect to the variable t , or it can only be obtained by discrete data with errors, then we should apply the regularization technique based on the smoothing spline model [21]. \tilde{r} , \tilde{u} and \tilde{f} are approximation solutions of the exact functions r , u and f , respectively.

Based on the inverse heat conduction problems proposed in [21], we will present the detailed algorithms for the one-dimensional (1-D) and two-dimensional (2-D) IHCPs in the rectangular domains, respectively. Simultaneously, the 2-D IHCP for the non-rectangular domain in the smooth boundary case, with the Neumann boundary conditions, will be studied in the following parts.

3.1. 1-D IHCP for the rectangular domain

We now consider 1-D IHCP with time-dependent heat source $f(t)$ being stated as follows

$$\frac{\partial u}{\partial t} = \frac{\partial^2 u}{\partial x^2} + f(t), \quad 0 < x < 1, \quad 0 < t \leq t_{\max}, \tag{3.15}$$

with the initial condition

$$u(x, 0) = u_0(x), \quad 0 \leq x \leq 1, \tag{3.16}$$

the Neumann boundary conditions

$$u_x(0, t) = s(t), \quad u_x(1, t) = l(t), \quad 0 \leq t \leq t_{\max}, \tag{3.17}$$

and the over-specification point x^* in the spatial domain $(0, 1)$ satisfying

$$u(x^*, t) = g(t), \quad 0 \leq t \leq t_{\max}, \tag{3.18}$$

where $u_0(x), s(t), l(t)$ and $g(t)$ are the given functions, the functions $u(x, t)$ and $f(t)$ are unknown. In addition, we suppose that the given functions satisfy the following compatibility conditions

$$u_0(x^*) = g(0), \quad (u_0)_x(0) = s(0), \quad (u_0)_x(1) = l(0).$$

The PDE-constrained optimization method obtained by the above Eqs. (3.1)–(3.9) is applied to problems (3.15)–(3.18), then we have

$$\begin{aligned} \tilde{\mathcal{L}}_{31}(\Lambda) = & \frac{1}{2} \left\{ \sum_{j=1}^{m_1} \left(\sum_{i=1}^N \alpha_i \phi_i(x_j^0, t_j^0) - u_0^\sigma(x_j^0) \right)^2 + \right. \\ & \sum_{j=1}^{m_2} \left(\sum_{i=1}^N \alpha_i \frac{\partial \phi_i}{\partial x}(x_j^1, t_j^1) - s^\sigma(t_j^1) \right)^2 + \\ & \left. \sum_{j=1}^{m_3} \left(\sum_{i=1}^N \alpha_i \frac{\partial \phi_i}{\partial x}(x_j^2, t_j^2) - l^\sigma(t_j^2) \right)^2 \right\}, \tag{3.19} \end{aligned}$$

where $M = m_1 + m_2 + m_3$. Moreover, the source points $\{x_i^s, t_i^s\}_{i=1}^N$ can be chosen as $\Theta_1 \cup \Theta_2 \cup \Theta_3$ by

$$\begin{aligned} \Theta_1 & := \{(x_i^s, t_i^s) : x_i^s = -d_1, 0 \leq t_i^s \leq t_{\max}, i = 1, \dots, n_1\}, \\ \Theta_2 & := \{(x_i^s, t_i^s) : 0 \leq x_i^s \leq 1, t_i^s = -\tau, i = n_1 + 1, \dots, n_1 + n_2\}, \\ \Theta_3 & := \{(x_i^s, t_i^s) : x_i^s = 1 + d_2, 0 \leq t_i^s \leq t_{\max}, i = n_1 + n_2 + 1, \dots, N\}, \end{aligned}$$

where $d_1, d_2, \tau > 0$ are fixed constants, and $n_3 = N - \sum_{i=1}^2 n_i$. Simultaneously, the collocation points $\{x_j^0, t_j^0\}_{j=1}^{m_1}$, $\{x_j^1, t_j^1\}_{j=1}^{m_2}$ and $\{x_j^2, t_j^2\}_{j=1}^{m_3}$ are chosen as follows

$$\begin{aligned} \Xi_1 & := \{(x_j^0, t_j^0) : 0 \leq x_j^0 \leq 1, t_j^0 = 0, j = 1, \dots, m_1\}, \\ \Xi_2 & := \{(x_j^1, t_j^1) : x_j^1 = 0, 0 \leq t_j^1 \leq t_{\max}, j = 1, \dots, m_2\}, \\ \Xi_3 & := \{(x_j^2, t_j^2) : x_j^2 = 1, 0 \leq t_j^2 \leq t_{\max}, j = 1, \dots, m_3\}. \end{aligned}$$

One can refer to [27,28] for the similar details. Furthermore, we get the following quadratic form

$$\tilde{\mathcal{L}}_{31}(\Lambda) = \frac{1}{2} \{ \Lambda'(A_1 + A_2 + A_3)\Lambda - 2\Lambda'(b_1 + b_2 + b_3) + C_1 + C_2 + C_3 \}, \tag{3.20}$$

where

$$\begin{cases} A_1 := [(A_1)_{i,k}] \in \mathbb{R}^{N \times N}, (A_1)_{i,k} = \sum_{j=1}^{m_1} \phi_i(x_j^0, t_j^0) \phi_k(x_j^0, t_j^0), \\ b_1 := [(b_1)_i] \in \mathbb{R}^N, (b_1)_i = \sum_{j=1}^{m_1} \phi_i(x_j^0, t_j^0) u_0^\sigma(x_j^0), \\ C_1 := \sum_{j=1}^{m_1} (u_0^\sigma(x_j^0))^2, \\ \\ A_2 := [(A_2)_{i,k}] \in \mathbb{R}^{N \times N}, (A_2)_{i,k} = \sum_{j=1}^{m_2} \frac{\partial \phi_i}{\partial x}(x_j^1, t_j^1) \frac{\partial \phi_k}{\partial x}(x_j^1, t_j^1), \\ b_2 := [(b_2)_i] \in \mathbb{R}^N, (b_2)_i = \sum_{j=1}^{m_2} \frac{\partial \phi_i}{\partial x}(x_j^1, t_j^1) s^\sigma(t_j^1), \\ C_2 := \sum_{j=1}^{m_2} (s^\sigma(t_j^1))^2, \\ \\ A_3 := [(A_3)_{i,k}] \in \mathbb{R}^{N \times N}, (A_3)_{i,k} = \sum_{j=1}^{m_3} \frac{\partial \phi_i}{\partial x}(x_j^2, t_j^2) \frac{\partial \phi_k}{\partial x}(x_j^2, t_j^2), \\ b_3 := [(b_3)_i] \in \mathbb{R}^N, (b_3)_i = \sum_{j=1}^{m_3} \frac{\partial \phi_i}{\partial x}(x_j^2, t_j^2) l^\sigma(t_j^2), \\ C_3 := \sum_{j=1}^{m_3} (l^\sigma(t_j^2))^2, \end{cases}$$

and $i, k = 1, 2, \dots, N$. By differentiating $\tilde{\mathcal{L}}_{31}$ of (3.20) with respect to Λ , and setting the derivatives to be zero, we can obtain the following system of equations by

$$\bar{A}\Lambda = \bar{b}, \quad (3.21)$$

where $\bar{A} = \sum_{i=1}^3 A_i$, $\bar{b} = \sum_{i=1}^3 b_i$. Due to the ill-posed nature of the IHCPs, the resulting matrix \bar{A} above is ill-conditioned, i.e., the condition number of \bar{A} is usually very large. Moreover, the right-hand side \bar{b} is a set of discrete data contaminated by inherent measurement noises, here we apply the Tikhonov regularization technique to obtain stable numerical solution by Eq. (3.21), and get

$$\Lambda_\beta^* := \arg \min_{\Lambda} \{ \|\bar{A}\Lambda - \bar{b}\|_2^2 + \beta^2 \|\Lambda\|_2^2 \}, \quad (3.22)$$

where $\beta > 0$ is an unknown regularization parameter. In the regularization tools, there are some classical criterions, such as the generalized cross-validation (GCV), the L -curve criterion, and the quasi-optimality criterion etc. to compute the value β . We choose a good regularization parameter β by using the GCV in this paper, more details can be referred to the literatures [21,33–35]. In addition, the Matlab code package, as a tool for choosing the parameter β , was developed by Hansen [36].

Thus, the approximation solutions $\tilde{u}(x, t)$, $\tilde{f}(t)$ can be computed by Eqs. (3.13) and (3.14), respectively.

3.2. 2-D IHCP for the rectangular domain

We will discuss 2-D IHCP with time-dependent heat source $f(t)$ in the rectangular domain as

$$\frac{\partial u}{\partial t} = \frac{\partial^2 u}{\partial x^2} + \frac{\partial^2 u}{\partial y^2} + f(t), \quad 0 < x, y < 1, \quad 0 < t \leq t_{\max}, \quad (3.23)$$

with the initial condition

$$u(x, y, 0) = \varphi(x, y), \quad 0 \leq x, y \leq 1, \quad (3.24)$$

the Neumann boundary conditions

$$u_x(0, y, t) = f_1(y, t), \quad u_x(1, y, t) = f_3(y, t), \quad 0 \leq y \leq 1, \quad 0 \leq t \leq t_{\max}, \quad (3.25)$$

$$u_y(x, 0, t) = f_2(x, t), u_y(x, 1, t) = f_4(x, t), \quad 0 \leq x \leq 1, \quad 0 \leq t \leq t_{\max}, \quad (3.26)$$

and a pair of over-specification data (x^*, y^*) in the spatial domain $(0, 1) \times (0, 1)$ satisfying

$$u(x^*, y^*, t) = g(t), \quad 0 \leq t \leq t_{\max}, \quad (3.27)$$

where $\varphi(x, y), f_1(y, t), f_2(x, t), f_3(y, t), f_4(x, t)$ and $g(t)$ are given functions, which satisfy the following compatibility conditions

$$\begin{aligned} f_1(y, 0) &= \varphi_x(0, y), \quad f_3(y, 0) = \varphi_x(1, y), \\ f_2(x, 0) &= \varphi_y(x, 0), \quad f_4(x, 0) = \varphi_y(x, 1), \quad \varphi(x^*, y^*) = g(0), \end{aligned}$$

where $0 \leq x \leq 1, 0 \leq y \leq 1$, but $u(x, y, t)$ and $f(t)$ are unknown.

Similarly to the above case of 1-D IHCP, we can obtain the following form by using the PDE-constrained optimization method obtained by Eqs. (3.1)–(3.9)

$$\begin{aligned} \tilde{\mathcal{L}}_{32}(\Lambda) &= \frac{1}{2} \left\{ \sum_{j=1}^{m_1} \left(\sum_{i=1}^N \alpha_i \phi_i(x_j^0, y_j^0, t_j^0) - \varphi^\sigma(x_j^0, y_j^0) \right)^2 + \right. \\ &\quad \sum_{j=1}^{m_2} \left(\sum_{i=1}^N \alpha_i \frac{\partial \phi_i}{\partial x}(x_j^1, y_j^1, t_j^1) - f_1^\sigma(y_j^1, t_j^1) \right)^2 + \\ &\quad \sum_{j=1}^{m_3} \left(\sum_{i=1}^N \alpha_i \frac{\partial \phi_i}{\partial x}(x_j^2, y_j^2, t_j^2) - f_3^\sigma(y_j^2, t_j^2) \right)^2 + \\ &\quad \sum_{j=1}^{m_4} \left(\sum_{i=1}^N \alpha_i \frac{\partial \phi_i}{\partial y}(x_j^3, y_j^3, t_j^3) - f_2^\sigma(x_j^3, t_j^3) \right)^2 + \\ &\quad \left. \sum_{j=1}^{m_5} \left(\sum_{i=1}^N \alpha_i \frac{\partial \phi_i}{\partial y}(x_j^4, y_j^4, t_j^4) - f_4^\sigma(x_j^4, t_j^4) \right)^2 \right\}, \quad (3.28) \end{aligned}$$

where $M = \sum_{i=1}^5 m_i$. The source points $\{x_i^s, y_i^s, t_i^s\}_{i=1}^N$ located outside the physical domain are given by

$$\begin{aligned} \Theta_1 &:= \{(x_i^s, y_i^s, t_i^s) : 0 \leq x_i^s \leq 1, 0 \leq y_i^s \leq 1, t_i^s = -\tau, i = 1, \dots, n_1\}, \\ \Theta_2 &:= \{(x_i^s, y_i^s, t_i^s) : x_i^s = -d_4, 0 \leq y_i^s \leq 1, 0 \leq t_i^s \leq t_{\max}, \\ &\quad i = n_1 + 1, \dots, n_1 + n_2\}, \\ \Theta_3 &:= \{(x_i^s, y_i^s, t_i^s) : x_i^s = 1 + d_3, 0 \leq y_i^s \leq 1, 0 \leq t_i^s \leq t_{\max}, \\ &\quad i = n_1 + n_2 + 1, \dots, n_1 + n_2 + n_3\}, \\ \Theta_4 &:= \{(x_i^s, y_i^s, t_i^s) : 0 \leq x_i^s \leq 1, y_i^s = -d_2, 0 \leq t_i^s \leq t_{\max}, \\ &\quad i = n_1 + n_2 + n_3 + 1, \dots, n_1 + n_2 + n_3 + n_4\}, \\ \Theta_5 &:= \{(x_i^s, y_i^s, t_i^s) : 0 \leq x_i^s \leq 1, y_i^s = 1 + d_1, 0 \leq t_i^s \leq t_{\max}, \\ &\quad i = n_1 + n_2 + n_3 + n_4 + 1, \dots, N\}, \end{aligned}$$

where the parameters $\tau, d_1, d_2, d_3, d_4 > 0$ are constants, and $n_5 = N - \sum_{i=1}^4 n_i$. Furthermore, the collocation points $\{x_j^0, y_j^0, t_j^0\}_{j=1}^{m_1}, \{x_j^1, y_j^1, t_j^1\}_{j=1}^{m_2}, \{x_j^2, y_j^2, t_j^2\}_{j=1}^{m_3}, \{x_j^3, y_j^3, t_j^3\}_{j=1}^{m_4}, \{x_j^4, y_j^4, t_j^4\}_{j=1}^{m_5}$

are chosen as follows

$$\begin{aligned}\Xi_1 &:= \{(x_j^0, y_j^0, t_j^0) : 0 \leq x_j^0 \leq 1, 0 \leq y_j^0 \leq 1, t_j^0 = 0, j = 1, \dots, m_1\}, \\ \Xi_2 &:= \{(x_j^1, y_j^1, t_j^1) : x_j^1 = 0, 0 \leq y_j^1 \leq 1, 0 \leq t_j^1 \leq t_{\max}, j = 1, \dots, m_2\}, \\ \Xi_3 &:= \{(x_j^2, y_j^2, t_j^2) : x_j^2 = 1, 0 \leq y_j^2 \leq 1, 0 \leq t_j^2 \leq t_{\max}, j = 1, \dots, m_3\}, \\ \Xi_4 &:= \{(x_j^3, y_j^3, t_j^3) : 0 \leq x_j^3 \leq 1, y_j^3 = 0, 0 \leq t_j^3 \leq t_{\max}, j = 1, \dots, m_4\}, \\ \Xi_5 &:= \{(x_j^4, y_j^4, t_j^4) : 0 \leq x_j^4 \leq 1, y_j^4 = 1, 0 \leq t_j^4 \leq t_{\max}, j = 1, \dots, m_5\}.\end{aligned}$$

According to Eq. (3.28), we can obtain the following quadratic problem with respect to Λ by

$$\begin{aligned}\tilde{\mathcal{L}}_{32}(\Lambda) &= \frac{1}{2} \{ \Lambda' (Q_1 + Q_2 + Q_3 + Q_4 + Q_5) \Lambda - 2 \Lambda' (h_1 + h_2 + h_3 + h_4 + h_5) + \\ &\quad \hat{C}_1 + \hat{C}_2 + \hat{C}_3 + \hat{C}_4 + \hat{C}_5 \},\end{aligned}\tag{3.29}$$

where

$$\begin{cases} Q_1 := [(Q_1)_{i,k}] \in \mathbb{R}^{N \times N}, (Q_1)_{i,k} = \sum_{j=1}^{m_1} \phi_i(x_j^0, y_j^0, t_j^0) \phi_k(x_j^0, y_j^0, t_j^0), \\ h_1 := [(h_1)_i] \in \mathbb{R}^N, (h_1)_i = \sum_{j=1}^{m_1} \phi_i(x_j^0, y_j^0, t_j^0) \varphi^\sigma(x_j^0, y_j^0), \\ \hat{C}_1 := \sum_{j=1}^{m_1} (\varphi^\sigma(x_j^0, y_j^0))^2, \\ \\ Q_2 := [(Q_2)_{i,k}] \in \mathbb{R}^{N \times N}, (Q_2)_{i,k} = \sum_{j=1}^{m_2} \frac{\partial \phi_i}{\partial x}(x_j^1, y_j^1, t_j^1) \frac{\partial \phi_k}{\partial x}(x_j^1, y_j^1, t_j^1), \\ h_2 := [(h_2)_i] \in \mathbb{R}^N, (h_2)_i = \sum_{j=1}^{m_2} \frac{\partial \phi_i}{\partial x}(x_j^1, y_j^1, t_j^1) f_1^\sigma(y_j^1, t_j^1), \\ \hat{C}_2 := \sum_{j=1}^{m_2} (f_1^\sigma(y_j^1, t_j^1))^2, \\ \\ Q_3 := [(Q_3)_{i,k}] \in \mathbb{R}^{N \times N}, (Q_3)_{i,k} = \sum_{j=1}^{m_3} \frac{\partial \phi_i}{\partial x}(x_j^2, y_j^2, t_j^2) \frac{\partial \phi_k}{\partial x}(x_j^2, y_j^2, t_j^2), \\ h_3 := [(h_3)_i] \in \mathbb{R}^N, (h_3)_i = \sum_{j=1}^{m_3} \frac{\partial \phi_i}{\partial x}(x_j^2, y_j^2, t_j^2) f_3^\sigma(y_j^2, t_j^2), \\ \hat{C}_3 := \sum_{j=1}^{m_3} (f_3^\sigma(y_j^2, t_j^2))^2, \\ \\ Q_4 := [(Q_4)_{i,k}] \in \mathbb{R}^{N \times N}, (Q_4)_{i,k} = \sum_{j=1}^{m_4} \frac{\partial \phi_i}{\partial y}(x_j^3, y_j^3, t_j^3) \frac{\partial \phi_k}{\partial y}(x_j^3, y_j^3, t_j^3), \\ h_4 := [(h_4)_i] \in \mathbb{R}^N, (h_4)_i = \sum_{j=1}^{m_4} \frac{\partial \phi_i}{\partial x}(x_j^3, y_j^3, t_j^3) f_2^\sigma(x_j^3, t_j^3), \\ \hat{C}_4 := \sum_{j=1}^{m_4} (f_2^\sigma(x_j^3, t_j^3))^2, \\ \\ Q_5 := [(Q_5)_{i,k}] \in \mathbb{R}^{N \times N}, (Q_5)_{i,k} = \sum_{j=1}^{m_5} \frac{\partial \phi_i}{\partial y}(x_j^4, y_j^4, t_j^4) \frac{\partial \phi_k}{\partial y}(x_j^4, y_j^4, t_j^4), \\ h_5 := [(h_5)_i] \in \mathbb{R}^N, (h_5)_i = \sum_{j=1}^{m_5} \frac{\partial \phi_i}{\partial x}(x_j^4, y_j^4, t_j^4) f_4^\sigma(x_j^4, t_j^4), \\ \hat{C}_5 := \sum_{j=1}^{m_5} (f_4^\sigma(x_j^4, t_j^4))^2,\end{cases}$$

and $i, k = 1, 2, \dots, N$. Similarly, by differentiating $\tilde{\mathcal{L}}_{32}$ of (3.29) with respect to Λ , and setting the derivatives to be zero, we can obtain a system of linear equations as follows

$$\bar{Q} \Lambda = \bar{h},\tag{3.30}$$

where $\bar{Q} = \sum_{i=1}^5 Q_i$, $\bar{h} = \sum_{i=1}^5 h_i$. The identified functions $\tilde{u}(x, y, t)$ and $\tilde{f}(t)$ can be obtained by Eqs. (3.13) and (3.14), combined with the Tikhonov regularization technique.

3.3. 2-D IHCP for the non-rectangular domain with smooth boundary

We now consider 2-D IHCP with time-dependent heat source $f(t)$ stated for non-rectangular domain with smooth boundary as follows

$$\frac{\partial u}{\partial t} = \frac{\partial^2 u}{\partial x^2} + \frac{\partial^2 u}{\partial y^2} + f(t), \quad (x, y) \in \Omega, \quad 0 < t \leq t_{\max}, \quad (3.31)$$

with the initial condition

$$u(x, y, 0) = \chi(x, y), \quad (x, y) \in \bar{\Omega}, \quad (3.32)$$

the Neumann boundary condition

$$\frac{\partial u}{\partial \bar{n}}(x, y, t) = u_N, \quad (x, y) \in \partial\Omega, \quad 0 \leq t \leq t_{\max}, \quad (3.33)$$

and a pair of over-specification data (x^*, y^*) in domain Ω , satisfying

$$u(x^*, y^*, t) = g(t), \quad 0 \leq t \leq t_{\max}, \quad (3.34)$$

where Ω is the non-rectangular domain with smooth boundary in \mathbb{R}^2 , u_N denotes the known and measured Neumann data, $\chi(x, y)$ and $g(t)$ are the given functions, but $u(x, y, t)$ and $f(t)$ are unknown.

By the PDE-constrained optimization method (3.1)–(3.9) above, we can derive the following formula

$$\begin{aligned} \tilde{\mathcal{L}}_{33}(\Lambda) = & \frac{1}{2} \left\{ \sum_{j=1}^{m_1} \left(\sum_{i=1}^N \alpha_i \phi_i(x_j^0, y_j^0, t_j^0) - \chi^\sigma(x_j^0, y_j^0) \right)^2 + \right. \\ & \left. + \sum_{j=m_1+1}^M \left(\sum_{i=1}^N \alpha_i \frac{\partial \phi_i}{\partial \bar{n}}(x_j^1, y_j^1, t_j^1) - u_N^\sigma(x_j^1, y_j^1, t_j^1) \right)^2 \right\}. \end{aligned} \quad (3.35)$$

The source points $\{x_i^s, y_i^s, t_i^s\}_{i=1}^N$ located outside physical domain $\Omega \times [0, t_{\max}]$ are given as follows

$$\begin{aligned} \Theta_1 := & \{(x_i^s, y_i^s, t_i^s) : (x_i^s, y_i^s) \in \bar{\Omega}, t_i^s = -\tau, i = 1, \dots, n_1\}, \\ \Theta_2 := & \{(x_i^s, y_i^s, t_i^s) : (x_i^s, y_i^s) \in \partial\tilde{\Omega}, 0 \leq t_i^s \leq t_{\max}, i = n_1 + 1, \dots, N\}, \end{aligned}$$

where $\tilde{\Omega} := \Omega \cup \Delta\Omega$, $\Delta\Omega$ denotes the outside expansion-domain of Ω , see Figure 1, $\tau > 0$ is a fixed constant, $n_2 = N - n_1$, and $m_2 = M - m_1$. We can make suitable setting according to the given different problems. Moreover, the collocation points $\{x_j^0, y_j^0, t_j^0\}_{j=1}^{m_1}$ and $\{x_j^1, y_j^1, t_j^1\}_{j=m_1+1}^M$ are devised by

$$\begin{aligned} \Xi_1 := & \{(x_j^0, y_j^0, t_j^0) : (x_j^0, y_j^0) \in \bar{\Omega}, t_j^0 = 0, j = 1, \dots, m_1\}, \\ \Xi_2 := & \{(x_j^1, y_j^1, t_j^1) : (x_j^1, y_j^1) \in \partial\Omega, 0 \leq t_j^1 \leq t_{\max}, j = m_1 + 1, \dots, M\}. \end{aligned}$$

The quadratic optimization problem can be obtained by Eq. (3.35) as follows

$$\tilde{\mathcal{L}}_{33}(\Lambda) = \frac{1}{2} \{ \Lambda'(Z_1 + Z_2)\Lambda - 2\Lambda'(q_1 + q_2) + \tilde{C}_1 + \tilde{C}_2 \}, \quad (3.36)$$

where

$$\begin{cases} Z_1 := [(Z_1)_{i,k}] \in \mathbb{R}^{N \times N}, \quad (Z_1)_{i,k} = \sum_{j=1}^{m_1} \phi_i(x_j^0, y_j^0, t_j^0) \phi_k(x_j^0, y_j^0, t_j^0), \\ q_1 := [(q_1)_i] \in \mathbb{R}^N, \quad (q_1)_i = \sum_{j=1}^{m_1} \phi_i(x_j^0, y_j^0, t_j^0) \chi^\sigma(x_j^0, y_j^0), \\ \tilde{C}_1 := \sum_{j=1}^{m_1} (\chi^\sigma(x_j^0, y_j^0))^2, \end{cases}$$

$$\begin{cases} Z_2 := [(Z_2)_{i,k}] \in \mathbb{R}^{N \times N}, & (Z_2)_{i,k} = \sum_{j=m_1+1}^M \frac{\partial \phi_i}{\partial n}(x_j^1, y_j^1, t_j^1) \frac{\partial \phi_k}{\partial n}(x_j^1, y_j^1, t_j^1), \\ q_2 := [(q_2)_i] \in \mathbb{R}^N, & (q_2)_i = \sum_{j=m_1+1}^M \frac{\partial \phi_i}{\partial n}(x_j^1, y_j^1, t_j^1) u_N^\sigma(x_j^1, y_j^1, t_j^1), \\ \tilde{C}_2 := \sum_{j=m_1+1}^M (u_N^\sigma(x_j^1, y_j^1, t_j^1))^2, \end{cases}$$

and $i, k = 1, 2, \dots, N$. Analogously, by differentiating $\tilde{\mathcal{L}}_{33}$ of (3.36) with respect to Λ , and setting the derivatives to be zero, we can obtain the following system of equations by

$$\bar{Z}\Lambda = \bar{q}, \tag{3.37}$$

where $\bar{Z} = \sum_{i=1}^2 Z_i$, and $\bar{q} = \sum_{i=1}^2 q_i$. According to Eqs. (3.13) and (3.14), combining with the Tikhonov regularization technique, we can obtain the approximation solutions $\tilde{u}(x, y, t)$ and $\tilde{f}(t)$ of $u(x, y, t)$ and $f(t)$, respectively.

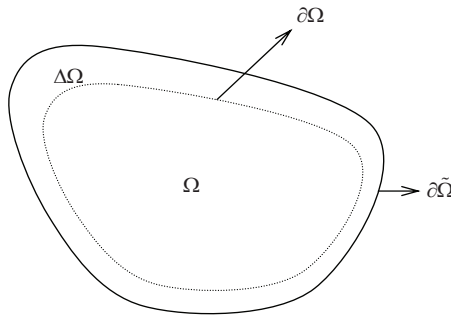


Figure 1 The plot of source domain $\partial\tilde{\Omega}$

4. Numerical tests

In order to test the efficiency of the proposed scheme, we replace the exact data of the original initial and Neumann boundary conditions by the measurement data contained noise level σ as follows

$$\varphi^\sigma(x) = \varphi(x)(1 + \sigma(2 \cdot \text{rand}() - 1)), \tag{4.1}$$

where $\text{rand}()$ is a pseudo-random value, which can be generated by using MATLAB `rand`. Similarly, other boundary functions are constructed as (4.1) in this section. In addition, to demonstrate the effectiveness of the proposed method in this paper, we compare with the numerical results of other methods in terms of approximation accuracy, computation time and stability, such as the method of fundamental solution raised by Wen [23] (denoted by MFS), the scheme of radial basis functions devised by Zhang and Li [21] (denoted by RBFs) and the multiquadric quasi-interpolation proposed by Chen and Wu [37,38] (denoted by MQQI).

In numerical computation, we consistently select the maximum time $t_{\max} = 1$, and employ uniform meshes in both spatial and temporal domains. $\beta(\cdot)$ denotes the regularization parameter of corresponding matrix, which can be obtained practically by GCV criterion and the manual correction. $CPU(s)$ indicates the total time for processing instructions of a computer program, and we define the unit of time by second (s). Furthermore, in order to show efficiency and

accuracy of the approximation solutions, we propose the root-mean-square (RMS) error E_2 , the maximum error E_∞ and \hat{E}_2 (the maximum value of the RMS errors) by the following forms

$$E_{2u}(t_j) = \left(\frac{1}{M} \sum_{i=1}^M |\tilde{u}(x_i, t_j) - u(x_i, t_j)|^2 \right)^{\frac{1}{2}}, \quad E_{\infty u}(t_j) = \max_{1 \leq i \leq M} |\tilde{u}(x_i, t_j) - u(x_i, t_j)|,$$

$$E_{2f} = \left(\frac{1}{N} \sum_{j=1}^N |\tilde{f}(t_j) - f(t_j)|^2 \right)^{\frac{1}{2}}, \quad E_{\infty f} = \max_{1 \leq j \leq N} |\tilde{f}(t_j) - f(t_j)|, \quad \hat{E}_{2u} = \max_{1 \leq j \leq N} \{E_{2u}(t_j)\}.$$

Example 4.1 We consider 1-D IHCP for the rectangular domain, the exact solution of problem (3.15)–(3.18) is given by

$$u(x, t) = \exp(-t) \sin(x) - \frac{1}{2}tx^2 - \frac{1}{24}x^4,$$

$$f(t) = t.$$

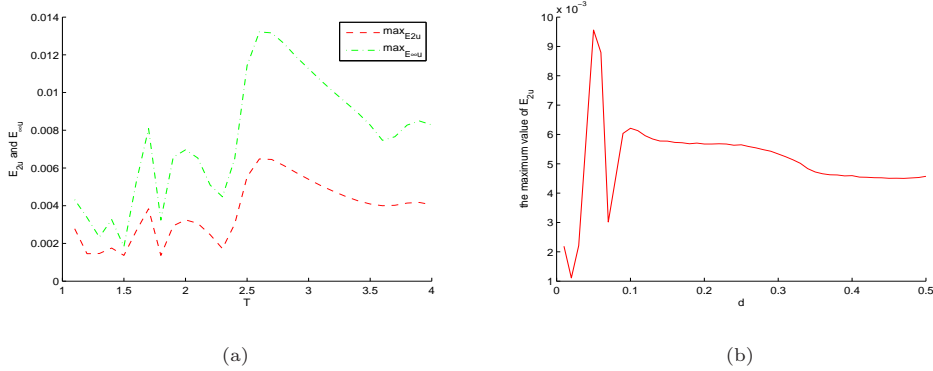


Figure 2 The plot (a) of the maximum E_{2u} , $E_{\infty u}$ corresponding to the constant $T \in [1.1, 4]$; the plot (b) of \hat{E}_{2u} with respect to the constant d , where the parameters $\{d_j\}_{j=1}^2 = d$ and $d \in [0.01, 0.5]$ in Example 4.1

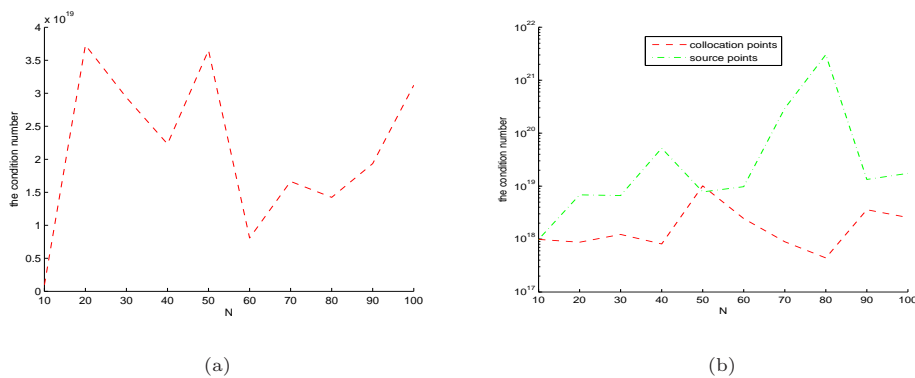


Figure 3 The condition number of resultant matrix with respect to the number N of the collocation points and source points: (a) the parameters $\{m_i\}_{i=1}^3 = \{n_i\}_{i=1}^3 = N$; (b) the parameters $\{m_i\}_{i=1}^3 = N$, $\{n_i\}_{i=1}^3 = 10$ in red, and $\{n_i\}_{i=1}^3 = N$, $\{m_i\}_{i=1}^3 = 10$ in green, $10 \leq N \leq 100$, for Example 4.1

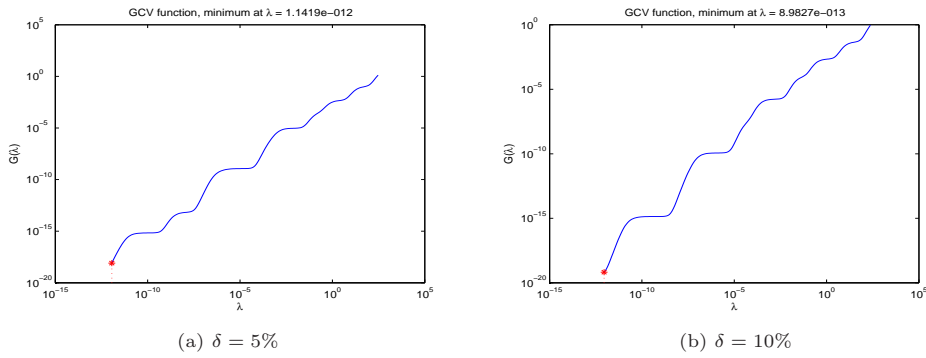


Figure 4 The plots of GCV function $G(\lambda)$ with respect to the regularization parameter λ , the noise levels (a) $\sigma = 5\%$ and (b) $\sigma = 10\%$ are added to the measured data in Example 4.1

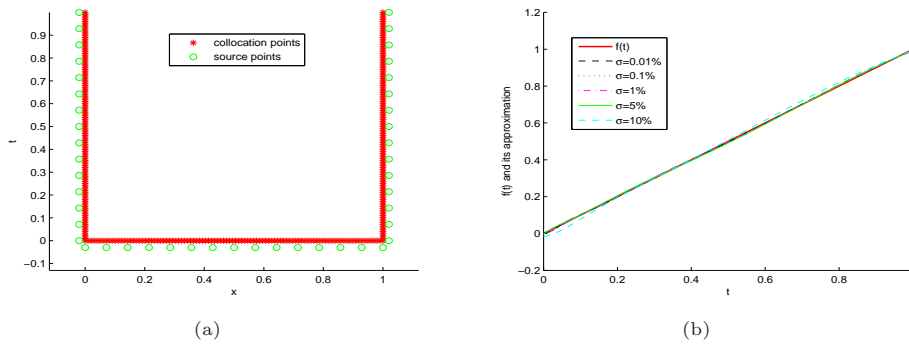


Figure 5 The 2-D distribution plot (a) of collocation points and source points, the exact function $f(t)$ and its approximation (b) with five different noise levels added to the measured data, where $\sigma = 0.01\%$, $\sigma = 0.1\%$, $\sigma = 1\%$, $\sigma = 5\%$ and $\sigma = 10\%$ in Example 4.1

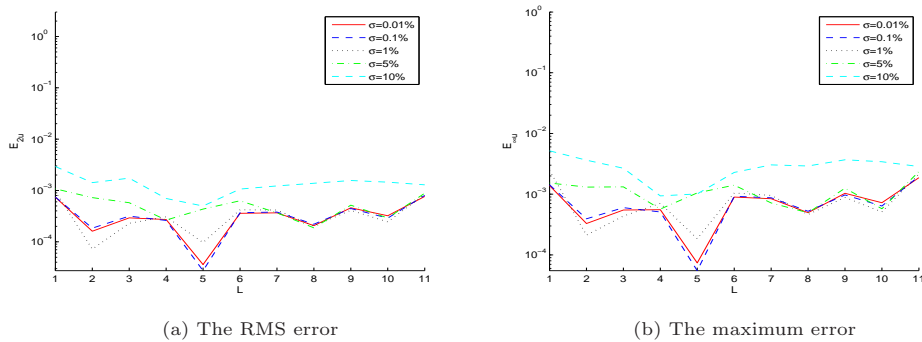


Figure 6 The RMS error (a) of function $u(x, t)$ and its maximum error (b) with $t_{\max} = 1$, and five different noise levels added to the measured data, namely $\sigma = 0.01\%$, $\sigma = 0.1\%$, $\sigma = 1\%$, $\sigma = 5\%$ and $\sigma = 10\%$, in Example 4.1, L denotes time level corresponding to $t = 0, 0.1, \dots, 1$

In Figure 2 (a), the results display the maximum values of E_{2u} and $E_{\infty u}$ with respect to the constant T for all different time levels t_j , here, we take $m_i = 100$, $n_i = 15, i = 1, 2, 3$, let T be in the interval $[1.1, 4]$ and the noise level $\sigma = 5\%$, it is shown that the accuracy of the approximation solutions are dependent on the parameter T . Figure 2 (b) shows that the plot

of \hat{E}_{2u} with respect to the constant d for the case of noise level $\sigma = 5\%$, where the parameters $\{d_j\}_{j=1}^2 = d$ and $d \in [0.01, 0.5]$. In addition, the condition number of resultant matrix \bar{A} is related to the total number of collocation (or source) points by Figure 3. It shows that the number N of the collocation points and source points is growing, i.e., $\{m_i\}_{i=1}^3 = \{n_i\}_{i=1}^3 = N$ in Figure 3 (a), it can be seen that the plot of the condition number of resultant matrix presents a fluctuant state, but not generally increase, where $10 \leq N \leq 100$. From Figure 3 (b), it can be demonstrated that the condition number of \bar{A} becomes larger, as the number N of source points is growing, but this effect is not obvious when the number of collocation points becomes bigger. Thus, we take consistently $x^* = 0.40$, $d_1 = d_2 = 0.02$, $\tau = 0.03$, $m_i = 100$ and $n_i = 15, i = 1, 2, 3$, moreover, the condition numbers of \bar{A} lie in the range of $10^{17} - 10^{19}$, for five different noise levels added to the measured data, namely $\sigma = 0.01\%, \sigma = 0.1\%, \sigma = 1\%, \sigma = 5\%$ and $\sigma = 10\%$ in Example 4.1. Figure 4 shows that the plots of GCV function $G(\lambda)$ with respect to the regularization parameter λ , which has the same meaning as the above $\beta(\cdot)$, while two noise levels are added to the measured valued, namely $\sigma = 5\%$ and $\sigma = 10\%$, respectively. In Figure 4 (a), $\lambda = 1.14 \times 10^{-12}$ for the case of $\sigma = 5\%$, and in Figure 4 (b), $\lambda = 8.98 \times 10^{-13}$ for the case of $\sigma = 10\%$. The 2-D distribution of the collocation and source points is represented by Figure 5 (a). According to Figures 5 (b), 6 (a)-(b) and Table 3, the numerical results are given to show that the proposed scheme is accurate and faster, it is shown that the computation time of CPU presented by [21] requires 2 times more than our technique in Table 3.

$n \backslash m$	10	20	30	40	50	60
10	9.86×10^{17}	8.73×10^{17}	1.22×10^{18}	8.08×10^{17}	1.01×10^{19}	2.44×10^{18}
20	6.85×10^{18}	3.73×10^{19}	2.12×10^{19}	4.17×10^{18}	2.07×10^{19}	9.06×10^{18}
30	6.64×10^{18}	1.54×10^{19}	2.93×10^{19}	4.38×10^{19}	1.18×10^{19}	9.89×10^{18}
40	5.21×10^{19}	1.35×10^{19}	1.18×10^{19}	2.23×10^{19}	6.13×10^{19}	5.98×10^{18}
50	7.79×10^{18}	2.54×10^{20}	1.05×10^{19}	1.02×10^{19}	3.65×10^{19}	7.76×10^{18}
60	9.77×10^{18}	1.46×10^{20}	1.07×10^{19}	4.82×10^{18}	1.20×10^{19}	8.07×10^{18}

Table 1 The condition number of coefficient matrix with respect to the numbers of collocation points and source points, where $\{m_i\}_{i=1}^3 = m, \{n_i\}_{i=1}^3 = n$ respectively, in Example 4.1

$n \backslash m$	10	20	30	40	50	60
10	1.12×10^{-2}	6.37×10^{-3}	2.09×10^{-3}	1.48×10^{-3}	1.65×10^{-3}	3.68×10^{-3}
20	1.11×10^{-2}	8.26×10^{-3}	2.76×10^{-3}	2.58×10^{-3}	1.70×10^{-3}	2.69×10^{-3}
30	1.42×10^{-2}	7.87×10^{-3}	2.36×10^{-3}	3.09×10^{-3}	2.33×10^{-3}	2.65×10^{-3}
40	9.13×10^{-3}	1.48×10^{-2}	1.83×10^{-3}	1.54×10^{-3}	2.97×10^{-3}	4.23×10^{-3}
50	9.86×10^{-3}	4.39×10^{-3}	3.63×10^{-3}	6.34×10^{-3}	4.18×10^{-3}	4.05×10^{-3}
60	6.11×10^{-3}	6.74×10^{-3}	3.81×10^{-3}	2.13×10^{-3}	2.82×10^{-3}	2.87×10^{-3}

Table 2 The condition number of coefficient matrix with respect to the numbers of collocation points and source points, where $\{m_i\}_{i=1}^3 = m, \{n_i\}_{i=1}^3 = n$ respectively, in Example 4.1

	$\sigma = 0.01\%$	$\sigma = 0.1\%$	$\sigma = 1\%$	$\sigma = 5\%$	$\sigma = 10\%$
T	1.2	1.2	1.2	1.5	1.8
$CPU(s)$	38.79	38.12	38.25	38.01	39.12
E_{2f}	3.46×10^{-3}	3.43×10^{-3}	3.70×10^{-3}	4.87×10^{-3}	1.48×10^{-2}
$E_{\infty f}$	7.40×10^{-3}	7.71×10^{-3}	8.68×10^{-3}	8.89×10^{-3}	3.03×10^{-2}
$\beta(\bar{A})$	0.30×10^{-12}	0.30×10^{-12}	0.30×10^{-12}	1.14×10^{-12}	8.98×10^{-13}
$CPU(s)(RBFs)$	78.56	78.69	78.18	77.58	85.22
$E_{2f}(RBFs)$	8.57×10^{-4}	1.25×10^{-3}	6.98×10^{-3}	8.83×10^{-3}	3.76×10^{-2}
$E_{\infty f}(RBFs)$	1.56×10^{-3}	3.01×10^{-3}	1.24×10^{-2}	1.85×10^{-2}	9.33×10^{-2}
$CPU(s)(MQQI)$	44.56	48.64	47.61	47.13	46.26
$E_{2f}(MQQI)$	5.65×10^{-2}	4.06×10^{-2}	5.67×10^{-2}	5.62×10^{-2}	5.82×10^{-2}
$E_{\infty f}(MQQI)$	7.17×10^{-2}	8.33×10^{-2}	7.47×10^{-2}	7.16×10^{-2}	9.82×10^{-2}

Table 3 The results of T , $CPU(s)$, E_{2f} , $E_{\infty f}$ and $\beta(\bar{A})$ with various error levels, namely $\sigma = 0.01\%$, $\sigma = 0.1\%$, $\sigma = 1\%$, $\sigma = 5\%$ and $\sigma = 10\%$ in Example 4.1, compared with the results of [21,37,38]

Example 4.2 The exact solution of problem (3.15)–(3.18) is given by

$$u(x, t) = x^2 + 2t + \sin(2\pi t),$$

$$f(t) = 2\pi \cos(2\pi t).$$

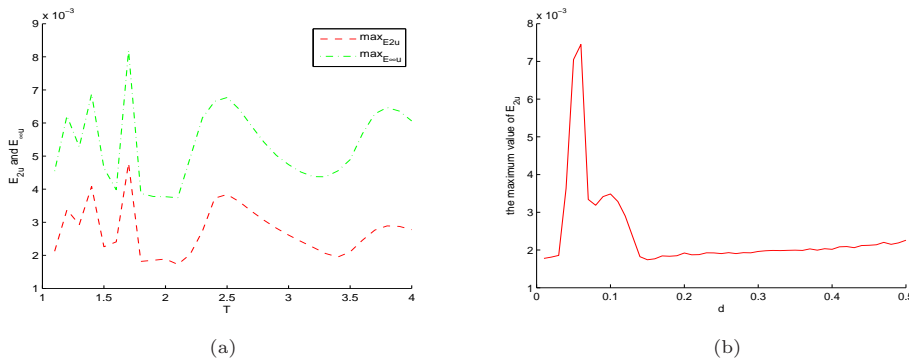


Figure 7 The plot (a) of the maximum E_{2u} , $E_{\infty u}$ corresponding to the constant $T \in [1.1, 4]$; the plot (b) of \hat{E}_{2u} with respect to the constant d , where the parameters $\{d_j\}_{j=1}^2 = d$ and $d \in [0.01, 0.5]$ in Example 4.2

Similar to Example 4.1, it is shown that the accuracy of approximation solutions is related to the constant T by Figure 7 (a), in this case, we take $m_i = 100$, $n_i = 10$ and the noise level $\sigma = 5\%$, where $i = 1, 2, 3$. Figure 7 (b) shows the plot of \hat{E}_{2u} with respect to d for the case of noise level $\sigma = 5\%$, namely $\{d_j\}_{j=1}^2 = d$, $d \in [0.01, 0.5]$. Figure 8 shows the condition number of coefficient matrix with respect to the number N of the collocation points and source points. By Figure 8 (a), as number N of the points is growing, the plot of the condition number of resultant matrix displays fluctuant, but generally does not increase. In Figure 8 (b), we obtain the analogous conclusion to Example 4.1 above, with the growing of the total number of source points, the change of the condition number becomes more obvious than the case of collocation points. Tables

4 and 5 show the condition numbers of coefficient matrix and the numerical results of \hat{E}_{2u} , with respect to the numbers of the collocation points and source points, respectively. Further, we take consistently $x^* = 0.25$, $d_1 = d_2 = 0.02$, $\tau = 0.03$, $m_i = 100$ and $n_i = 10, i = 1, 2, 3$, moreover, the condition numbers of \bar{A} lie between $10^{17} - 10^{18}$, for five different noise levels added to the measured data, namely $\sigma = 0.01\%, \sigma = 0.1\%, \sigma = 1\%, \sigma = 5\%$ and $\sigma = 10\%$ in Example 4.2. In Figure 9, the plots of GCV function $G(\lambda)$ with respect to the regularization parameter λ , when different noise levels $\sigma = 5\%$ and $\sigma = 10\%$ are added to the measured data. In Figure 9 (a), $\lambda = 0.60 \times 10^{-12}$ for the case of $\sigma = 5\%$, and in Figure 9 (b), $\lambda = 0.60 \times 10^{-12}$ for the case of $\sigma = 10\%$. The locations of collocation and source points are shown in Figure 10 (a). Combined with the numerical results of Example 4.1, the proposed technique is effective and quite satisfactory by Figures 10 (b), 11 (a)-(b) and Table 6. Moreover, the running time of CPU obtained by [21] is 3 times more than our scheme in Table 6. According to the approximation solutions of $f(t)$ in Tables 3 and 6, our provided technique is more robust to solve 1-D IHCPs, since the regularization parameters $\beta(\bar{A})$ are only needed to choose very small values and remain basically unchanged to obtain good numerical results, for five different noise levels added to the measured data.

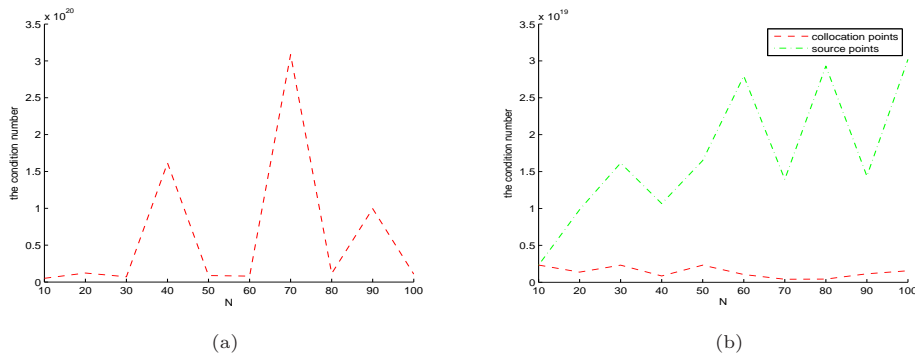


Figure 8 The condition number of resultant matrix with respect to the number N of the collocation points and source points: (a) the parameters $\{m_i\}_{i=1}^3 = \{n_i\}_{i=1}^3 = N$; (b) the parameters $\{m_i\}_{i=1}^3 = N, \{n_i\}_{i=1}^3 = 10$ in red, and $\{n_i\}_{i=1}^3 = N, \{m_i\}_{i=1}^3 = 10$ in green, $10 \leq N \leq 100$, for Example 4.2

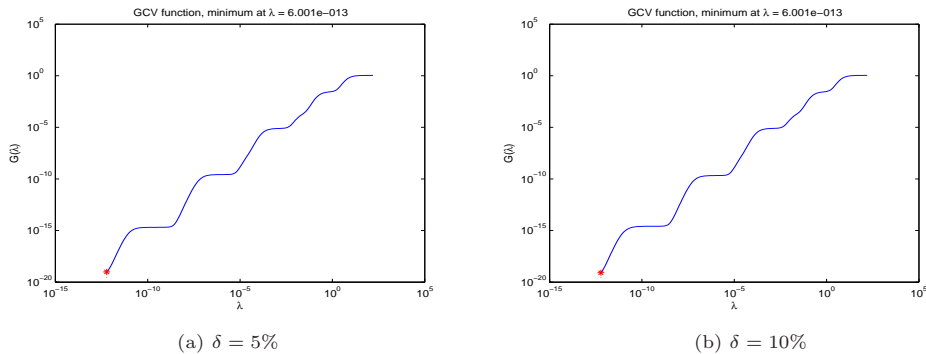


Figure 9 The plots of GCV function $G(\lambda)$ with respect to the regularization parameter λ , the noise levels (a) $\sigma = 5\%$ and (b) $\sigma = 10\%$ are added to the measured data in Example 4.2

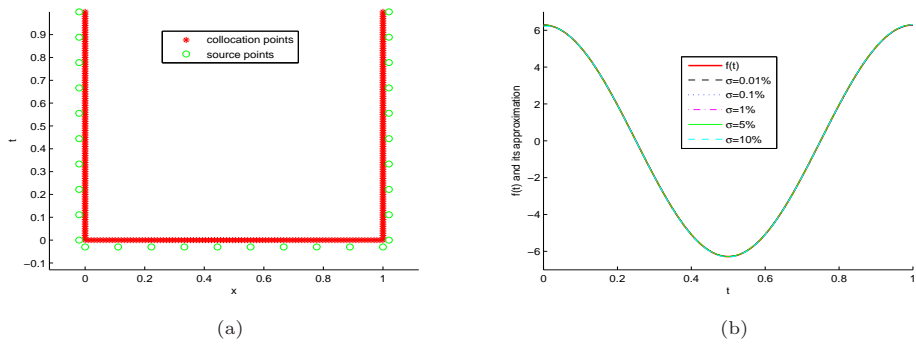


Figure 10 The 2-D distribution plot (a) of collocation points and source points, the exact function $f(t)$ and its approximation (b) with five different noise levels added to the measured data, where $\sigma = 0.01\%$, $\sigma = 0.1\%$, $\sigma = 1\%$, $\sigma = 5\%$ and $\sigma = 10\%$ in Example 4.2

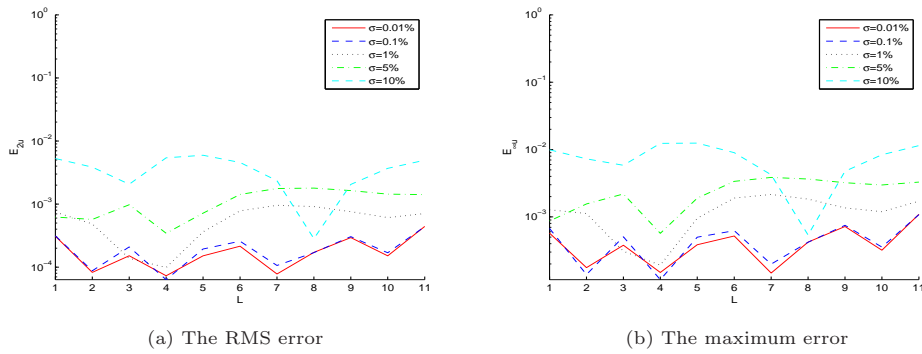


Figure 11 The RMS error (a) of function $u(x, t)$ and its maximum error (b) with $t_{\max} = 1$, and five different noise levels added to the measured data, namely $\sigma = 0.01\%$, $\sigma = 0.1\%$, $\sigma = 1\%$, $\sigma = 5\%$ and $\sigma = 10\%$, in Example 4.2, L denotes time level corresponding to $t = 0, 0.1, \dots, 1$

$m \backslash n$	10	20	30	40	50	60
10	5.00×10^{18}	3.93×10^{18}	4.53×10^{17}	1.14×10^{18}	1.12×10^{19}	1.62×10^{18}
20	7.91×10^{18}	1.22×10^{19}	7.63×10^{18}	1.36×10^{18}	2.73×10^{18}	6.53×10^{17}
30	4.17×10^{18}	8.33×10^{18}	7.05×10^{18}	9.19×10^{18}	1.63×10^{19}	1.09×10^{19}
40	3.30×10^{19}	9.30×10^{18}	7.19×10^{18}	1.62×10^{20}	4.54×10^{18}	1.08×10^{19}
50	3.67×10^{19}	6.39×10^{19}	1.49×10^{19}	7.12×10^{19}	8.81×10^{18}	1.03×10^{19}
60	2.47×10^{19}	4.06×10^{20}	3.57×10^{19}	5.27×10^{18}	1.82×10^{19}	8.00×10^{18}

Table 4 The condition number of coefficient matrix with respect to the numbers of collocation points and source points, where $\{m_i\}_{i=1}^3 = m, \{n_i\}_{i=1}^3 = n$ respectively, in Example 4.2

$n \backslash m$	10	20	30	40	50	60
10	2.56×10^{-2}	5.07×10^{-3}	8.10×10^{-3}	1.56×10^{-3}	6.43×10^{-3}	4.55×10^{-3}
20	1.53×10^{-2}	8.93×10^{-3}	7.57×10^{-3}	4.04×10^{-3}	3.32×10^{-3}	3.60×10^{-3}
30	1.61×10^{-2}	1.01×10^{-2}	2.04×10^{-3}	4.26×10^{-3}	1.64×10^{-3}	4.52×10^{-3}
40	6.58×10^{-3}	1.20×10^{-2}	2.82×10^{-3}	6.47×10^{-3}	4.75×10^{-3}	5.18×10^{-3}
50	1.66×10^{-2}	9.36×10^{-3}	6.53×10^{-3}	7.39×10^{-3}	6.93×10^{-3}	2.00×10^{-3}
60	1.54×10^{-2}	9.37×10^{-3}	1.13×10^{-2}	5.38×10^{-3}	3.80×10^{-3}	7.19×10^{-3}

Table 5 The results of \hat{E}_{2u} with respect to the numbers of collocation points and source points, where $\{m_i\}_{i=1}^3 = m, \{n_i\}_{i=1}^3 = n$ respectively, in Example 4.2

	$\sigma = 0.01\%$	$\sigma = 0.1\%$	$\sigma = 1\%$	$\sigma = 5\%$	$\sigma = 10\%$
T	1.5	1.5	1.5	1.8	1.8
$CPU(s)$	23.75	22.23	22.58	22.97	23.32
E_{2f}	2.61×10^{-3}	2.66×10^{-3}	4.13×10^{-3}	5.87×10^{-3}	1.82×10^{-2}
$E_{\infty f}$	7.63×10^{-3}	7.60×10^{-3}	2.00×10^{-2}	1.51×10^{-2}	7.80×10^{-2}
$\beta(\bar{A})$	0.50×10^{-12}	0.50×10^{-12}	0.50×10^{-12}	0.60×10^{-12}	0.60×10^{-12}
$CPU(s)(RBFs)$	85.07	84.57	85.05	84.06	99.05
$E_{2f}(RBFs)$	1.74×10^{-3}	1.81×10^{-3}	7.09×10^{-3}	9.89×10^{-3}	3.04×10^{-2}
$E_{\infty f}(RBFs)$	1.18×10^{-2}	1.43×10^{-2}	5.28×10^{-2}	8.85×10^{-2}	1.79×10^{-1}
$CPU(s)(MQQI)$	44.49	42.26	39.54	39.37	41.38
$E_{2f}(MQQI)$	3.18×10^{-1}	2.32×10^{-1}	2.33×10^{-1}	2.41×10^{-1}	2.47×10^{-1}
$E_{\infty f}(MQQI)$	6.75×10^{-1}	4.68×10^{-1}	4.72×10^{-1}	5.53×10^{-1}	5.92×10^{-1}

Table 6 The results of $T, CPU(s), E_{2f}, E_{\infty f}$ and $\beta(\bar{A})$ with various error levels, namely $\sigma = 0.01\%, \sigma = 0.1\%, \sigma = 1\%, \sigma = 5\%$ and $\sigma = 10\%$ in Example 4.2, compared with the results of [21,37,38]

Example 4.3 We consider the following exact solution of 2-D IHCPs, including Case 1. (3.23)–(3.27) and Case 2. (3.31)–(3.34), is given by

$$u(x, y, t) = \exp(-t)(\sin x + \cos y) + t^2 - \frac{t^3}{2},$$

$$f(t) = 2t - \frac{3t^2}{2}.$$

In Example 4.3, we should propose the above problems involving some different physical domains (such as the rectangular domain and the non-rectangular domain with smooth boundary) to demonstrate the effectiveness of the presented schemes. Compared with the accuracy of numerical results obtained by using the techniques of [21,23], including the computation time, there are two types of the non-rectangular domain (the Circular-domain and the Peanut-domain) to be developed as investigated objects.

Domain type 1: Example 4.3 in the rectangular domain

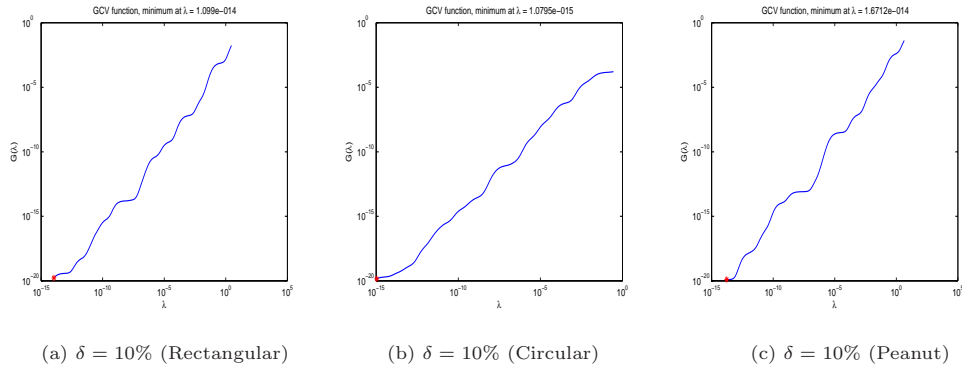


Figure 12 The plots of GCV function $G(\lambda)$ with respect to the regularization parameter λ , when the noise level $\sigma = 10\%$ is added to the measured data of three different domains: (a) the Rectangular-domain case, (b) the Circular -domain case, (c) the Peanut-domain case in Example 4.3

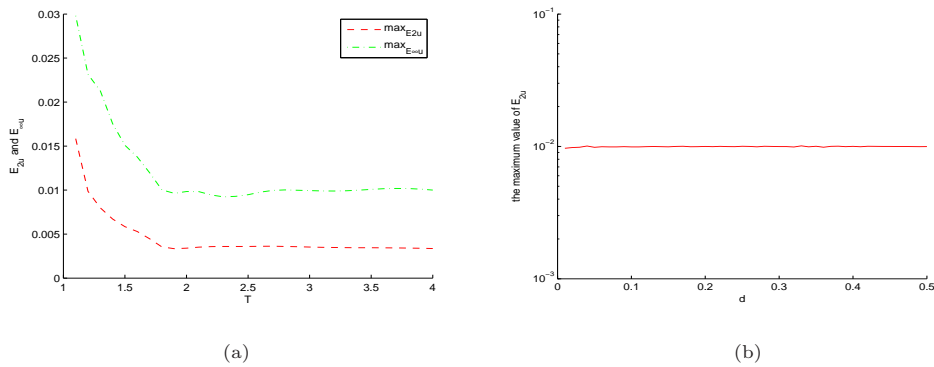


Figure 13 The plot (a) of the maximum E_{2u} , $E_{\infty u}$ corresponding to the constant $T \in [1.1, 4]$; the plot (b) of \hat{E}_{2u} with respect to the constant d , where the parameters $\{d_j\}_{j=1}^4 = d$ and $d \in [0.01, 0.5]$, for the rectangular domain case of Example 4.3

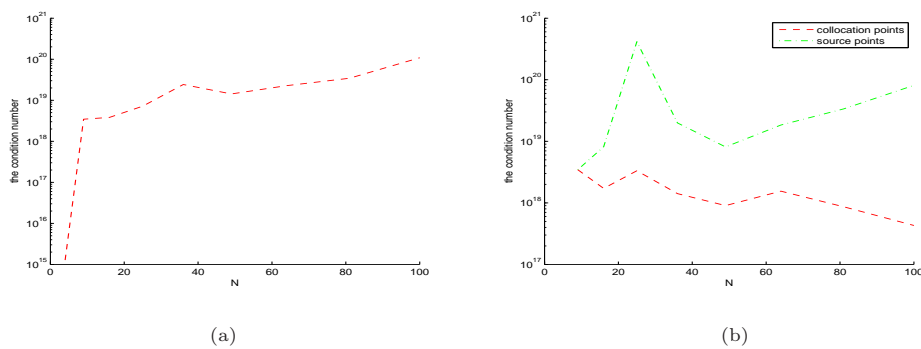


Figure 14 The condition number of resultant matrix with respect to the number N of the collocation points and source points: (a) the parameters $\{m_i\}_{i=1}^5 = \{n_i\}_{i=1}^5 = N$; (b) the parameters $\{m_i\}_{i=1}^5 = N, \{n_i\}_{i=1}^5 = 9$ in red, and $\{n_i\}_{i=1}^5 = N, \{m_i\}_{i=1}^5 = 9$ in green, $9 \leq N \leq 100$, for the rectangular domain case of Example 4.3

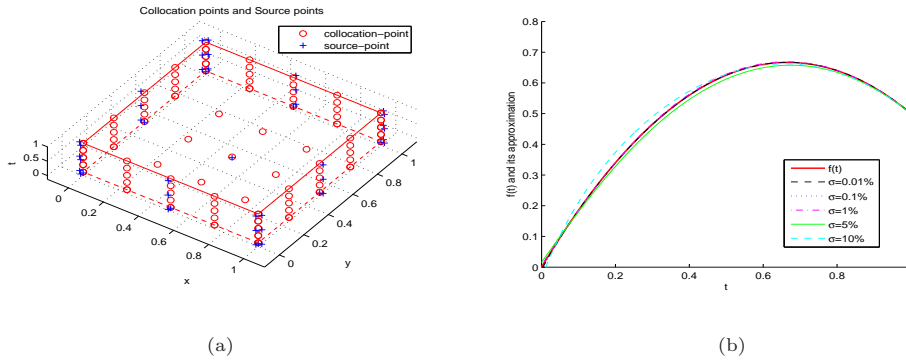


Figure 15 The 3-D distribution plot (a) of collocation points and source points, the exact function $f(t)$ and its approximation (b) with five different noise levels added to the measured data, where $\sigma = 0.01\%$, $\sigma = 0.1\%$, $\sigma = 1\%$, $\sigma = 5\%$ and $\sigma = 10\%$ for the rectangular domain case of Example 4.3

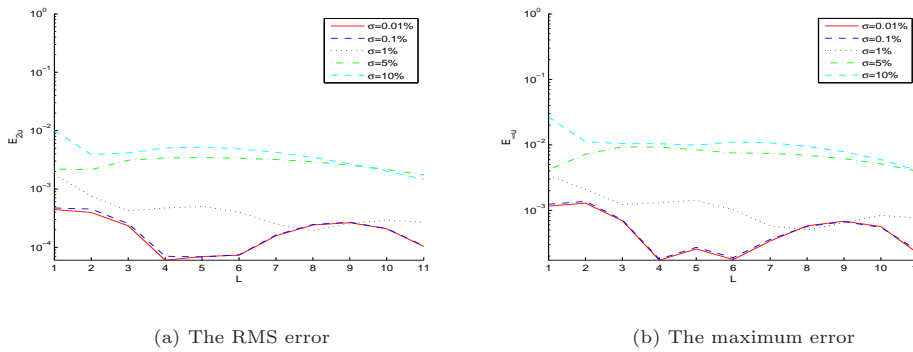


Figure 16 The RMS error (a) of function $u(x, y, t)$ and its maximum error (b) with $t_{\max} = 1$, and five different noise levels added to the measured data, namely $\sigma = 0.01\%$, $\sigma = 0.1\%$, $\sigma = 1\%$, $\sigma = 5\%$ and $\sigma = 10\%$, for the rectangular domain case of Example 4.3, L denotes time level corresponding to $t = 0, 0.1, \dots, 1$

$m \backslash n$	9	16	25	36	49	64
9	2.60×10^{-2}	8.43×10^{-3}	8.75×10^{-3}	8.60×10^{-3}	8.47×10^{-3}	6.05×10^{-3}
16	2.79×10^{-2}	1.25×10^{-2}	1.70×10^{-2}	5.99×10^{-3}	5.52×10^{-3}	5.78×10^{-3}
25	6.54×10^{-2}	1.56×10^{-2}	1.09×10^{-2}	5.05×10^{-3}	1.23×10^{-2}	6.45×10^{-3}
36	6.72×10^{-2}	1.13×10^{-2}	1.25×10^{-2}	1.33×10^{-2}	7.10×10^{-3}	6.50×10^{-3}
49	3.39×10^{-2}	1.25×10^{-2}	1.64×10^{-2}	1.26×10^{-2}	1.12×10^{-2}	4.00×10^{-3}
64	2.12×10^{-2}	1.04×10^{-2}	1.35×10^{-2}	8.79×10^{-3}	1.18×10^{-2}	6.19×10^{-3}

Table 7 The results of \hat{E}_{2u} with respect to the numbers of collocation points and source points, where $\{m_i\}_{i=1}^5 = m$, $\{n_i\}_{i=1}^5 = n$, respectively, for the rectangular domain case of Example 4.3

	$\sigma = 0.01\%$	$\sigma = 0.1\%$	$\sigma = 1\%$	$\sigma = 5\%$	$\sigma = 10\%$
T	1.5	1.5	1.5	2.0	2.0
$CPU(s)$	20.06	19.81	19.90	19.93	19.50
E_{2f}	1.16×10^{-3}	1.18×10^{-3}	2.15×10^{-3}	9.94×10^{-3}	1.67×10^{-2}
$E_{\infty f}$	8.54×10^{-3}	7.79×10^{-3}	4.83×10^{-3}	1.57×10^{-2}	3.44×10^{-2}
$\beta(\bar{Q})$	0.10×10^{-12}	0.10×10^{-12}	0.10×10^{-12}	0.30×10^{-12}	0.11×10^{-13}
$CPU(s)(RBFs)$	19.92	19.90	19.99	19.87	20.18
$E_{2f}(RBFs)$	1.07×10^{-3}	1.61×10^{-3}	2.46×10^{-3}	1.04×10^{-2}	1.27×10^{-2}
$E_{\infty f}(RBFs)$	3.36×10^{-3}	4.64×10^{-3}	9.31×10^{-3}	3.53×10^{-2}	7.74×10^{-2}
$CPU(s)(MFS)$	35.75	35.94	37.00	36.86	36.79
$E_{2f}(MFS)$	8.92×10^{-4}	1.92×10^{-3}	6.71×10^{-3}	1.44×10^{-2}	1.80×10^{-2}
$E_{\infty f}(MFS)$	2.55×10^{-3}	1.03×10^{-2}	4.47×10^{-2}	4.99×10^{-2}	4.40×10^{-2}
$CPU(s)(MQQI)$	92.35	94.07	92.86	93.52	93.60
$E_{2f}(MQQI)$	2.72×10^{-2}	2.73×10^{-2}	2.07×10^{-2}	2.80×10^{-2}	8.42×10^{-2}
$E_{\infty f}(MQQI)$	3.55×10^{-2}	3.55×10^{-2}	3.04×10^{-2}	3.60×10^{-2}	9.51×10^{-2}

Table 8 The results of T , $CPU(s)$, E_{2f} , $E_{\infty f}$ and $\beta(\bar{Q})$ with various error levels, namely $\sigma = 0.01\%$, $\sigma = 0.1\%$, $\sigma = 1\%$, $\sigma = 5\%$ and $\sigma = 10\%$ for the rectangular domain case of Example 4.3, compared with the results of [21,23,37,38]

The plots of GCV function $G(\lambda)$ are proposed in Figure 12, with respect to the regularization parameter λ . The maximum values of E_{2u} , $E_{\infty u}$ are dependent on the choice of T in the interval [1.1, 2], but it is unobvious that the change of approximation solutions are related to the value T in the domain [2, 4] by Figure 13 (a), where $m_i = 25$, $n_i = 9$, $i = 1, \dots, 5$ in Eqs. (3.28) and (3.29), and the noise level $\sigma = 5\%$. Similarly, the condition number has been greater impact on the number of source points by Figure 14 (b), so we take consistently $x^* = y^* = 0.5$, $m_i = 25$, $n_i = 9$, $d_j = 0.02$ and $\tau = 0.03$, where $i = 1, \dots, 5$, $j = 1, \dots, 4$. Furthermore, the condition numbers of resultant matrix \bar{Q} lie between $10^{17} - 10^{18}$. In Figure 15 (a) describes the distribution of collocation and source points. It is shown that the presented scheme is accurate and quite satisfactory by Figures 15 (b), 16 (a)-(b) and Table 8.

Domain type 2: Example 4.3 in the non-rectangular domain with smooth boundary

In this part, we present two types of the non-rectangular domain with smooth boundary, such as the Circular-domain and the Peanut-domain respectively, to investigate 2-D IHCPs with the Neumann boundary condition corresponding to the subsection 3.3 in this paper. The following Circular-domain is given in [21]

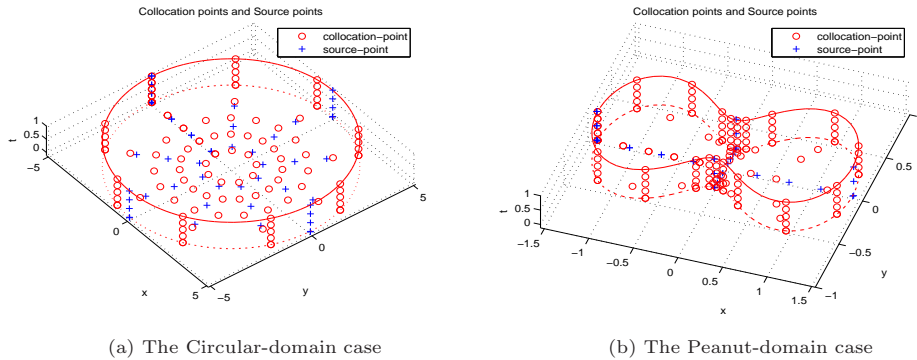
$$\partial\Omega = \{(x, y, t) : x = \rho \cos(\theta), y = \rho \sin(\theta), 0 \leq t \leq t_{\max}, \rho > 0, -\pi \leq \theta \leq \pi\}, \quad (4.2)$$

and the Peanut-domain is obtained as follows [21,39]

$$\partial\Omega = \{(x, y, t) : x = \rho(\theta) \cos(\theta), y = \rho(\theta) \sin(\theta), 0 \leq t \leq t_{\max}, -\pi \leq \theta \leq \pi\}, \quad (4.3)$$

where

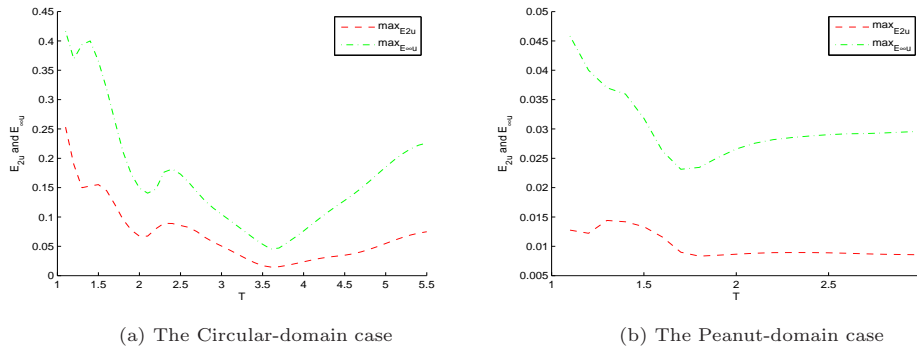
$$\rho(\theta) = (\cos(2\theta) + \sqrt{1.1 - \sin^2(2\theta)})^{\frac{1}{2}}.$$



(a) The Circular-domain case

(b) The Peanut-domain case

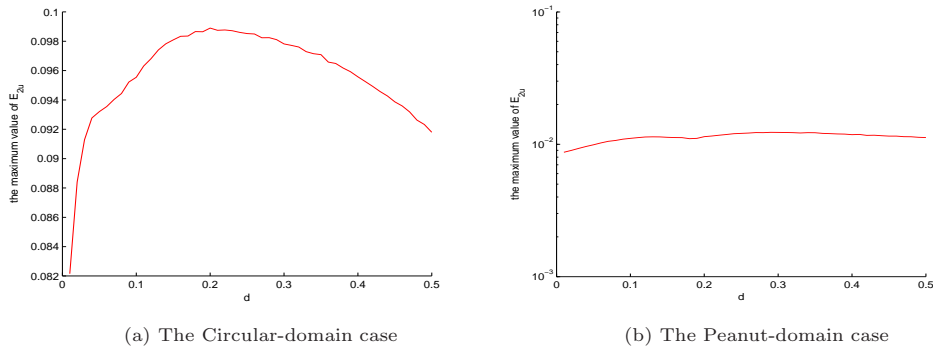
Figure 17 The 3-D distribution plots of collocation points and source points for the non-rectangular of Example 4.3



(a) The Circular-domain case

(b) The Peanut-domain case

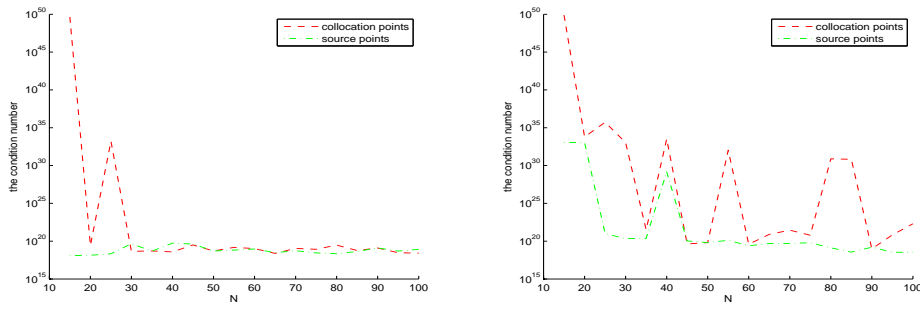
Figure 18 The plots of the maximum E_{2u} , $E_{\infty u}$ corresponding to the constant T for the non-rectangular of Example 4.3



(a) The Circular-domain case

(b) The Peanut-domain case

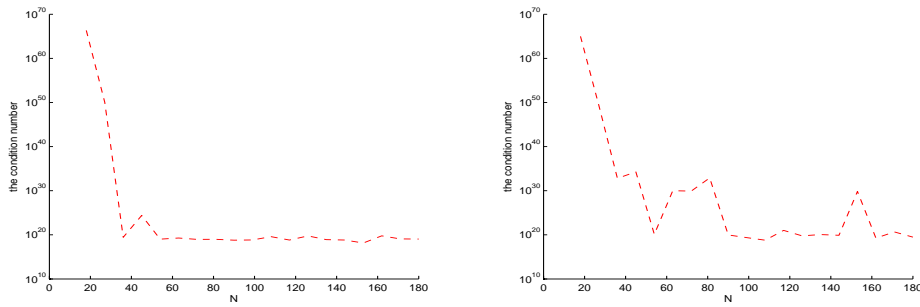
Figure 19 The plots of \hat{E}_{2u} with respect to the constant d , where the parameters $\{d_1\} = d$ and $d \in [0.01, 0.5]$, for the non-rectangular of Example 4.3



(a) The Circular-domain case

(b) The Peanut-domain case

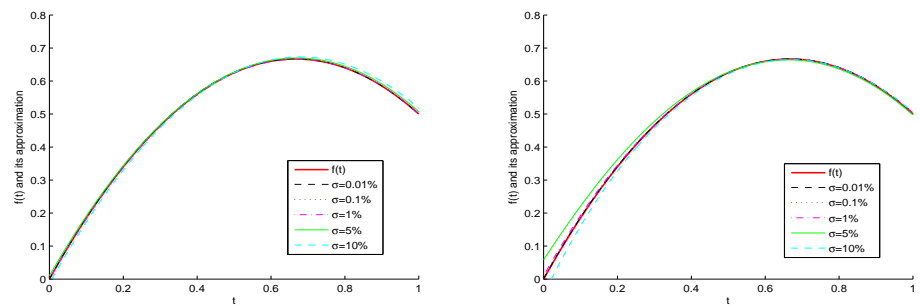
Figure 20 The condition number of resultant matrix with respect to the number of collocation points and source points: (a) $\sum_{i=1}^2 m_i = N$, $\sum_{i=1}^2 n_i = 50$ in red, and $\sum_{i=1}^2 n_i = N$, $\sum_{i=1}^2 m_i = 50$ in green; (b) $\sum_{i=1}^2 m_i = N$, $\sum_{i=1}^2 n_i = 50$ in red, and $\sum_{i=1}^2 n_i = N$, $\sum_{i=1}^2 m_i = 50$ in green, where $15 \leq N \leq 100$, for the non-rectangular of Example 4.3



(a) The Circular-domain case

(b) The Peanut-domain case

Figure 21 The condition number of resultant matrix with respect to the numbers of the collocation points and source points, i.e., $\sum_{i=1}^2 (m_i + n_i) = N$ ($18 \leq N \leq 180$), for the non-rectangular of Example 4.3



(a) The Circular-domain case

(b) The Peanut-domain case

Figure 22 The exact function $f(t)$ and its approximation with five different noise levels added to the measured data, where $\sigma = 0.01\%$, $\sigma = 0.1\%$, $\sigma = 1\%$, $\sigma = 5\%$ and $\sigma = 10\%$ for the non-rectangular domain of Example 4.3

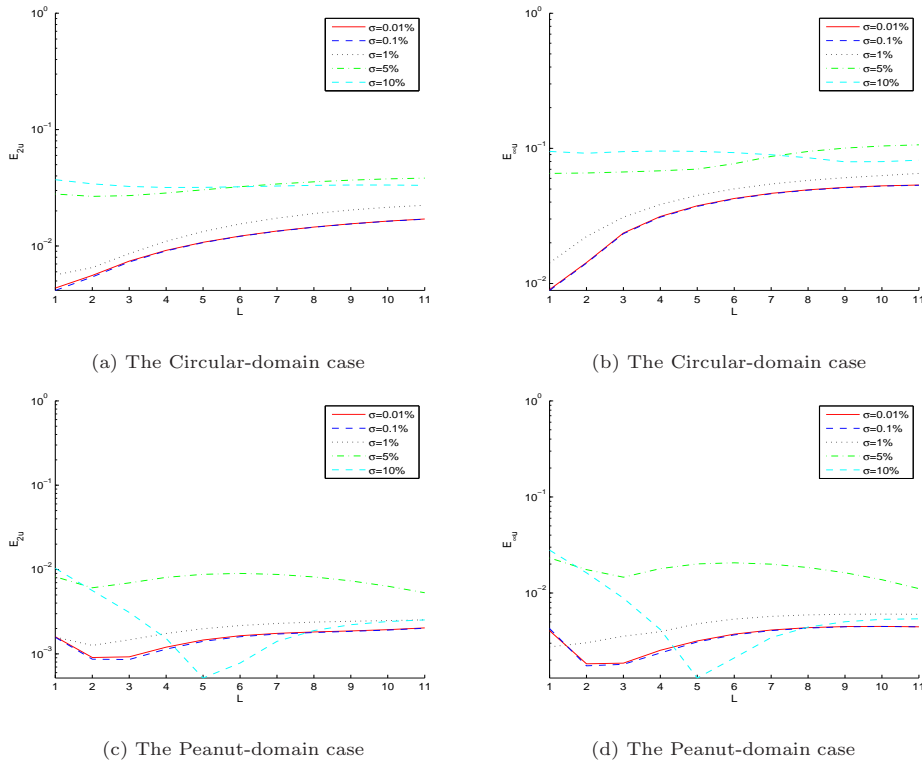


Figure 23 The RMS error of function $u(x, y, t)$ and its maximum error with $t_{\max} = 1$, and five different noise levels added to the measured data, namely $\sigma = 0.01\%$, $\sigma = 0.1\%$, $\sigma = 1\%$, $\sigma = 5\%$ and $\sigma = 10\%$, for the non-rectangular domain of Example 4.3, L denotes time level corresponding to $t = 0, 0.1, \dots, 1$

		M						
		N	30	50	70	90	110	130
Cir.	25		1.03×10^{-1}	1.87×10^{-1}	1.09×10^{-1}	6.25×10^{-2}	8.21×10^{-2}	7.15×10^{-2}
	45		8.48×10^{-2}	7.92×10^{-2}	1.93×10^{-2}	3.43×10^{-2}	2.69×10^{-2}	2.31×10^{-2}
	65		1.45×10^{-1}	1.66×10^{-1}	6.07×10^{-2}	3.14×10^{-2}	2.89×10^{-2}	4.51×10^{-2}
	85		1.86×10^{-1}	2.13×10^{-1}	7.63×10^{-2}	2.45×10^{-2}	4.09×10^{-2}	5.03×10^{-2}
	105		2.33×10^{-1}	2.15×10^{-1}	4.36×10^{-2}	2.88×10^{-2}	6.71×10^{-2}	2.44×10^{-2}
	125		1.82×10^{-1}	1.86×10^{-1}	5.15×10^{-2}	5.79×10^{-2}	4.06×10^{-2}	2.47×10^{-2}
Pea.	25		1.93×10^{-2}	1.53×10^{-2}	7.10×10^{-3}	8.44×10^{-3}	1.21×10^{-2}	1.34×10^{-2}
	40		2.13×10^{-2}	1.44×10^{-2}	1.52×10^{-2}	6.23×10^{-3}	1.16×10^{-2}	1.02×10^{-2}
	55		1.36×10^{-2}	1.15×10^{-2}	1.13×10^{-2}	6.48×10^{-3}	1.07×10^{-2}	1.09×10^{-2}
	70		1.64×10^{-2}	1.51×10^{-2}	1.16×10^{-2}	1.49×10^{-2}	9.91×10^{-3}	1.25×10^{-2}
	85		1.92×10^{-2}	1.40×10^{-2}	2.35×10^{-2}	2.48×10^{-2}	1.03×10^{-2}	1.31×10^{-2}
	100		2.73×10^{-2}	1.18×10^{-2}	2.02×10^{-2}	1.48×10^{-2}	8.10×10^{-3}	1.07×10^{-2}

Table 9 The results of \hat{E}_{2u} with respect to the numbers of collocation points $\sum_{i=1}^2 m_i = M$, and source points $\sum_{i=1}^2 n_i = N$, in the Circular-domain (called Cir.) and the Peanut-domain (called Pea.) settings, respectively, for Example 4.3

	$\sigma = 0.01\%$	$\sigma = 0.1\%$	$\sigma = 1\%$	$\sigma = 5\%$	$\sigma = 10\%$
T	3.5	3.5	4.0	4.4	5.0
$CPU(s)$	43.81	43.84	44.05	44.22	45.33
E_{2f}	1.08×10^{-3}	7.55×10^{-4}	1.54×10^{-3}	4.46×10^{-3}	9.66×10^{-3}
$E_{\infty f}$	1.60×10^{-3}	1.16×10^{-3}	2.29×10^{-3}	1.01×10^{-2}	1.76×10^{-2}
$\beta(\bar{Z})$	0.10×10^{-12}	0.10×10^{-12}	0.50×10^{-12}	0.50×10^{-12}	0.50×10^{-13}
Cir. $CPU(s)$ (RBFs)	39.84	35.89	34.59	35.45	34.37
E_{2f} (RBFs)	3.18×10^{-3}	7.32×10^{-3}	5.11×10^{-3}	2.33×10^{-2}	2.83×10^{-2}
$E_{\infty f}$ (RBFs)	7.34×10^{-3}	2.02×10^{-2}	3.61×10^{-2}	4.90×10^{-2}	8.69×10^{-2}
$CPU(s)$ (MFS)	72.63	67.24	67.00	66.63	78.94
E_{2f} (MFS)	5.56×10^{-3}	4.17×10^{-3}	1.16×10^{-2}	4.41×10^{-2}	3.40×10^{-2}
$E_{\infty f}$ (MFS)	1.76×10^{-2}	1.43×10^{-2}	2.24×10^{-2}	7.54×10^{-2}	4.14×10^{-2}
T	2.1	2.1	2.1	1.7	2.1
$CPU(s)$	33.19	32.66	32.73	32.78	33.89
E_{2f}	1.41×10^{-3}	1.49×10^{-3}	3.90×10^{-3}	1.86×10^{-2}	1.35×10^{-2}
$E_{\infty f}$	3.52×10^{-3}	3.48×10^{-3}	9.77×10^{-3}	5.84×10^{-2}	4.91×10^{-2}
$\beta(\bar{Z})$	0.30×10^{-12}	0.30×10^{-12}	0.10×10^{-12}	0.10×10^{-12}	0.17×10^{-13}
Pea. $CPU(s)$ (RBFs)	41.06	43.25	41.49	42.10	43.20
E_{2f} (RBFs)	3.48×10^{-3}	3.46×10^{-3}	1.18×10^{-2}	2.78×10^{-2}	4.50×10^{-2}
$E_{\infty f}$ (RBFs)	5.65×10^{-3}	9.23×10^{-3}	7.37×10^{-2}	8.09×10^{-2}	2.20×10^{-1}
$CPU(s)$ (MFS)	66.69	66.74	68.60	68.17	72.98
E_{2f} (MFS)	5.03×10^{-4}	1.41×10^{-3}	1.01×10^{-2}	1.72×10^{-2}	2.70×10^{-2}
$E_{\infty f}$ (MFS)	1.21×10^{-3}	1.09×10^{-2}	5.83×10^{-2}	7.64×10^{-2}	6.65×10^{-2}

Table 10 The results of T , $CPU(s)$, E_{2f} , $E_{\infty f}$ and $\beta(\bar{Z})$ with various error levels, namely $\sigma = 0.01\%$, $\sigma = 0.1\%$, $\sigma = 1\%$, $\sigma = 5\%$ and $\sigma = 10\%$ for Example 4.3, in the Circular-domain (called Cir.) and the Peanut-domain (called Pea.) settings, compared with the results of [21,23], respectively

Figure 17 shows that the 3-D distribution plots of the collocation points and source points for two types of the non-rectangular domain of Example 4.3. Similarly, it is known that the accuracy of desired approximation solutions is dependent on the selection of T by Figure 18. In Figure 20, the condition number of resultant matrices can be changed with the increasing number of collocation points (or source points). In this paper, we take $\rho = 5$, $x^* = 5 \cos(\frac{\pi}{3})$, $y^* = 5 \sin(\frac{\pi}{3})$, $\tau = 0.02$, the number of the boundary collocation points $M = 120$, and the number of the source points $N = 55$, the condition numbers of matrix \bar{Z} lie between $10^{18} - 10^{19}$ in the Circular-domain setting. Analogously, we take $x^* = \rho(\frac{\pi}{3}) \cos(\frac{\pi}{3})$, $y^* = \rho(\frac{\pi}{3}) \sin(\frac{\pi}{3})$, $\tau = 0.02$, the number of the collocation points $M = 153$, and the number of the source points $N = 35$, all the condition numbers of \bar{Z} are 10^{20} in the peanut-domain case. According to Figures 22, 23 and Table 10, the numerical results developed by the proposed techniques are accurate and effective.

In addition, Figures 2 (b), 7 (b), 13 (b) and 19 show the plots of \hat{E}_{2u} with respect to the constant d , we can see that the approximation solutions $\tilde{u}(x, t)$ of $u(x, t)$ are stable and effective, and the accuracy orders remain basically unchanged for selecting any small $d_j > 0$ on certain interval. According to Figures 3 (a), 8 (a), 14 (a), 21, and Tables 1, 2, 4, 5, 7, 9, the condition

numbers of resultant matrix and the numerical results of \hat{E}_{2u} are presented, with respect to the numbers of the collocation points and source points, and we consistently take the case of the noise level $\sigma = 5\%$. Further, when the numbers of the collocation points and source points increase, we note that the condition numbers not always become bigger.

In general, compared with the results of numerical examples in literatures [21,23], including $CPU(s)$ and the computation accuracy, the presented schemes are more robust and stable. Since there are several constants (such as T , the number of collocation points, etc.) to be determined in our presented methods, we only compute the total computation time of algorithms, but not include the time cost for selecting these values. All desired parameters are given in advance, and all programs are running in Intel's I7-3520M CPU @ 2.90GHz in this paper.

5. Conclusions

In this paper, we develop a general form of the PDE-constrained optimization method for solving IHCPs, with the time-dependent heat source term and Neumann boundary condition, which is an effective meshless numerical method. The approximation solution of identified temperature is constructed by using the fundamental solution as basis function. Since the resulting equations system is badly ill-conditioned, we apply the Tikhonov regularization technique with GCV criterion to obtain more stable numerical solutions. Meanwhile, due to the use of fundamental solution, the computation complexity can be reduced by avoiding computation of the Lagrange multiplier term. In practice, we can choose a few source points and more collocation points, to obtain effective and satisfactory numerical solutions. In addition, the proposed techniques are more robust by the above examples, since the regularization parameters β are selected very small values and remain basically unchanged to obtain good numerical results, when the noise level σ becomes bigger. However, it is our future work for the suitable choice of parameter T , and the ingenious design of collocation and source points in practical problems.

References

- [1] S. TAPASWINI, S. CHAKRAVERTY, D. BEHERA. *Numerical solution of the imprecisely defined inverse heat conduction problem*. Chin. Phys. B, 2015, **24**(5): 153–162.
- [2] D. A. POTER, K. E. EASTELING. *Phase Transformations in Metals and Alloys*. Chapman & Hall, London, 1981.
- [3] Y. C. HON, Ting WEI. *A Fundamental Solution Method for Inverse Heat Conduction Problem*. Eng. Ana. Bound. Elem., 2004, **28**(5): 489–495.
- [4] J. HADAMARD. *Lectures on Cauchy's problem in linear partial differential equations*. Yale University Press, New Haven, 1923.
- [5] Y. C. HON, Ting WEI. *The method of fundamental solution for solving multidimensional inverse heat conduction problems*. CMES: Comput. Model. Eng. Sci., 2005, **7**(2): 119–132.
- [6] D. N. HÀO, P. X. THANH, D. LESNIC, et al. *A boundary element method for multi-dimensional inverse heat conduction problem*. Int. J. Comput. Math., 2012, **89**: 1540–1554.
- [7] M. DEGHAN. *Parameter determination in a partial differential equation from the overspecified data*. Math. Comput. Modelling, 2005, **41**: 197–213.
- [8] K. KURPISZ, A. J. NOWAK. *BEM approach to inverse heat conduction problems*. Eng. Anal. Bound. Elem., 1992, **10**(4): 291–297.
- [9] D. LESNIC, L. ELLIOTT, D. B. INGHAM. *Application of the boundary element method to inverse heat conduction problems*. Int. J. Heat Mass Tran., 1996, **39**(7): 1503–1517.

- [10] Fajie WANG, Wen CHEN, Yan GU. *Boundary element analysis of inverse heat conduction problems in 2D thin-walled structures*. Int. J. Heat Mass Tran., 2015, **91**: 1001–1009.
- [11] A. H. D. CHENG, D. T. CHENG. *Heritage and early history of the boundary element method*. Eng. Anal. Bound. Elem., 2005, **29**(3): 268–302.
- [12] S. N. ATLURI, S. CHEN. *The Meshless Method*. Tech Science Press, Forsyth, 2002.
- [13] G. E. FASSHAUER. *Meshfree approximation methods with matlab*. Word Scientific Publishing Company, London, 2007.
- [14] Guangming YAO. *Local Radial Basis Function Methods for Solving Partial Differential Equations*. Dissertations & Theses-Gradworks, 2010.
- [15] M. D. BUHMANN. *Radial Basis Functions: Theory and Implementations*. Cambridge University Press, Cambridge, 2003.
- [16] W. CHEN, M. TANAKA. *A meshless, integration-free, and boundary-only RBF technique*. Comput. Math. Appl., 2002, **43**: 379–391.
- [17] M. DEGHAN, M. TATARI. *Determination of a control parameter in a one-dimensional parabolic equation using the method of radial basis functions*. Math. Comput. Modelling, 2006, **44**: 1160–1168.
- [18] Limin MA, Zongmin WU. *Radial basis functions method for parabolic inverse problem*. Int. J. Comput. Math., 2011, **88**(2): 384–395.
- [19] M. DEGHAN, V. MOHAMMADI. *The numerical solution of Cahn-Hilliard (CH) equation in one, two and three-dimensions via globally radial basis functions (GRBFs) and RBFs-differential quadrature (RBFs-DQ) methods*. Eng. Anal. Bound. Elem., 2015, **51**: 74–100.
- [20] M. ARGHAND, M. AMIRFAKHRIAN. *A meshless method based on the fundamental solution and radial basis function for solving an inverse heat conduction problem*. Adv. Math. Phys., **2015**: 1–8.
- [21] Yongfu ZHANG, Chongjun LI. *A Gaussian RBFs method with regularization for the numerical solution of inverse heat conduction problems*. Inverse Probl. Sci. Eng., 2016, **24**(9): 1606–1646.
- [22] Yan LIANG, Chuli FU, Fenglian YANG. *The method of fundamental solutions for the inverse heat source problem*. Eng. Ana. Bound. Elem., 2008, **32**: 216–222.
- [23] Jin WEN. *A meshless method for reconstructing the heat source and partial initial temperature in heat conduction*. Inverse Probl. Sci. Eng., 2011, **21**: 1007–1022.
- [24] A. KARAGEORGHIS, D. LESNIC, L. MARIN. *The method of fundamental solutions for an inverse boundary value problem in static thermo-elasticity*. Comput. Struct., 2014, **135**: 32–39.
- [25] V. D. KUPRADZE, M. A. ALEXIDZE. *The method of functional equations for the approximate solution of certain boundary value problems*. USSR Comput. Math. Phys., 1964, **4**: 82–126.
- [26] Bin CHEN, Wen CHEN, Xing WEI. *Characterization of space-dependent thermal conductivity for nonlinear functionally graded materials*. Int. J. Heat Mass Tran., 2015, **84**: 691–699.
- [27] Yao SUN. *A meshless method based on the method of fundamental solution for solving the steady-state heat conduction problems*. Int. J. Heat Mass Tran., 2016, **97**: 891–907.
- [28] S. S. ADAVAN, G. BIROS. *Multigrid algorithms for inverse problems with linear parabolic PDE constraints*. SIAM J. Sci. Comput., 2008, **31**(1): 369–397.
- [29] T. REES. *Preconditioning iterative methods for PDE constrained optimization*. DPhil Thesis, University of Oxford, 2010.
- [30] T. REES. *Optimal solving for PDE-constrained optimization*. SIAM. J. Sci. Comput., 2010, **32**(1): 271–298.
- [31] J. W. PEARSON. *A radial basis function method for solving PDE-constrained optimization*. Numer. Algorithms, 2013, **64**(3): 481–506.
- [32] P. MITIC, Y. F. RASHED. *Convergence and stability of the method of meshless fundamental solutions using an array of randomly distributed sources*. Eng. Anal. Bound. Elem., 2004, **28**:143–153.
- [33] P. CRAVEN, G. WAHBA. *Smoothing noisy data with spline functions*. Numer. Math., 1979, **31**: 377–403.
- [34] G. H. GOULB, M. HEATH, G. WAHBA. *Generalized Cross-Validation as a method for choosing a good ridge parameter*. Technometrics, 1979, **21**: 215–223.
- [35] G. WAHBA, J. WENDELBERGER. *Some new mathematical methods for variational objective analysis using splines and cross validation*. Monthly Weather Rev., 1980, **108**: 1122–1143.
- [36] P. C. HANSEN. *Regularization tools: A Matlab package for analysis and solution of discrete ill-posed problems*. Numer. Algorithms, 1994, **6**: 1–35.
- [37] Ronghua CHEN, Zongmin WU. *Applying multiquadric quasi-interpolation to solve Burgers' equation*. Appl. Math. Comput., 2006, **172**: 472–484.
- [38] Ronghua CHEN, Zongmin WU. *Solving partial differential equation by using multiquadric quasi-interpolation*. Appl. Math. Comput., 2007, **186**: 1502–1510.
- [39] Tongsong JIANG, Ming LI, C. S. CHEN. *The method of particular solutions for solving inverse problems of a nonhomogeneous convection-diffusion equation with variable coefficients*. Numerical Heat Transfer, Part A: Application, 2012, **61**: 338–352.